Numerical approximation based on deep convolutional neural network for high-dimensional fully nonlinear merged PDEs and 2BSDEs

Xu Xiao[a], Wenlin Qiu[*a], Omid Nikan[b]

[a]Key Laboratory of Computing and Stochastic Mathematics (Ministry of Education), School of Mathematics and Statistics, Hunan Normal University, Changsha, Hunan 410081, P. R. China
[b]School of Mathematics, Iran University of Science and Technology, Narmak, Tehran 16846-13114, Iran

Abstract

This paper proposes two efficient approximation methods to solve high-dimensional fully nonlinear partial differential equations (NPDEs) and second-order backward stochastic differential equations (2BSDEs), where such high-dimensional fully NPDEs are extremely difficult to solve because the computational cost of standard approximation methods grows exponentially with the number of dimensions. Therefore, we consider the following methods to overcome this difficulty. For the merged fully NPDEs and 2BSDEs system, combined with the time forward discretization and ReLU function, we use multi-scale deep learning fusion and convolutional neural network (CNN) techniques to obtain two numerical approximation schemes, respectively. Finally, three practical high-dimensional test problems involving Allen-Cahn, Black-Scholes-Barentblatt, and Hamiltonian-Jacobi-Bellman equations are given so that the first proposed method exhibits higher efficiency and accuracy than the existing method, while the second proposed method can extend the dimensionality of the completely NPDEs-2BSDEs system over 400 dimensions, from which the numerical results highlight the effectiveness of proposed methods.

Keywords: Convolutional neural network, ReLU, second-order backward stochastic differential equations, high-dimensional problems, Allen-Cahn equation, Black-Scholes-Barentblatt equation, Hamiltonian-Jacobi-Bellman equation, numerical experiments

2020 MSC: 65M22, 60H15, 65C30, 68T07

1. Introduction

Nonlinear Partial differential equations (NPDEs) play a key role in a large number of models, from finance to physics. Objects such as wave functions related to quantum physical systems, value functions which depict the fair prices of financial derivatives in pricing models, or value functions which depict the expected maximum utility in portfolio optimization problems that are usually presented as the solutions of NPDEs.

Roughly speaking, the non-linearity in PDEs used in financial engineering above is derived from the trade mix (the trade mix and utility of hedging financial derivatives claims in the case of the derivatives pricing problem must be maximized in the case of the portfolio optimization problem). The authors of [6, 29] adopted derivative pricing models with distinguishing lending rates. Crépey et al. [18] considered derivative pricing models incorporating the default risk of the issuer of the financial derivative. The authors of [3] proposed the models for the pricing of financial derivatives on untradable underlyings and analyzed, e.g., financial derivatives on the temperature or mortality-dependent financial derivatives. Amadori [1] considered the models incorporating that the trading strategy effects the price processes though the demand and supply.

The resulting PDEs from these models are usually high-dimensional, since the associated trading portfolio often involves a whole basket of financial assets (see [6, 18]). These high-dimensional NPDEs are often

exceedingly difficult to be solved approximately. Furthermore, due to the practical relevance of the afore-mentioned PDEs, there is a strong demand in the financial engineering industry to approximation solutions to such high-dimensional nonlinear parabolic PDEs.

There are lots of numerical approaches for solving parabolic NPDEs approximatively in the literature, from which, some of these methods are deterministic approximations, while others are stochastic approximations that depend on appropriate probabilistic representations of the corresponding PDE solutions, e.g., probabilistic representations in view of backward stochastic differential equations (BSDEs) (see [50, 51]), probabilistic representations in view of 2BSDEs (see [17]), probabilistic representations in view of branching diffusions (see [34]), and probabilistic representations in view of extensions of the classical Feynman-Kac formula (see [49]). Then, we can refer to some articles specifically, e.g., deterministic approximation approaches for PDEs (see [43, 54]), probabilistic approximation approaches for PDEs based on time discretizations of BSDEs (see [5, 6, 9, 13–16, 19–21, 24, 27–31, 36, 45–48, 53]), probabilistic approximation approaches for PDEs in view of suitable deep learning approximations for BSDEs (see [25, 33]), probabilistic approximation approaches for BSDEs in view of Wiener Chaos expansions (see [10]), probabilistic approximation approaches for BSDEs in view of sparse grid approximations (see [26]), probabilistic approximation approaches for PDEs based on branching diffusion representations (see [12, 34]), probabilistic approximation approaches for PDEs in view of time discretization of 2BSDEs (see [8, 17, 32, 40]), etc.

However, most of the above approximation techniques are only applicable when the dimension d of PDEs/BSDEs is quite small or only when there are strict constraints on the parameters or the type of PDEs considered (e.g., small nonlinearities, small terminal/initial conditions, the semi-linear structure of PDEs, etc). Therefore, to yield the numerical solutions of high-dimensional nonlinear PDEs, this is still an exceedingly difficult task, and there are only a few cases where practical algorithms for high-dimensional PDEs can be considered (see [22, 25, 33, 34]). Especially, to our knowledge, few practical algorithms for high-dimensional fully nonlinear parabolic PDEs currently exist in the scientific literature.

This paper intends to solve this difficulty and present new results, i.e., we solve the fully nonlinear merged PDEs and 2BSDEs with a new algorithm. Regarding the proposed problem, Beck et al. [4] first consider that by utilizing some properties from Peng's nonlinear expectation in high-dimensional space (see [52]). The proposed algorithm uses a connection between PDEs and 2BSDEs (see Cheridito et al. [17]) to yield a merged formulation of PDEs and 2BSDEs, whose approximated solutions can be obtained via combining time discretizations with a neural network (NN) based on deep learning (see [7, 11, 25, 33, 41–43, 54]). Loosely speaking, the merged formulation allows us to establish the original partial differential problem as a learning problem. The random loss function for the deep neural network in our method can be given by the error between the prescribed terminal condition of 2BSDEs and the neural network in view of forward time discretization of 2BSDEs. In fact, a corresponding deep-learning approximation algorithm for semilinear-type PDEs in view of forward BSDEs has been recently considered in [25, 33]. A crucial distinction between [25, 33] and our work is that herein we depend on the connection between fully nonlinear PDEs and 2BSDEs given in [17], while [25, 33] depend on the almost classical combination between PDEs and BSDEs (see [50, 51]). Besides, although Beck et al. [4] have considered the merged construction of fully nonlinear PDEs and 2BSDEs, there is still room for improvement. Under the limitation of computer memory, since they only consider linear neural networks, they can only calculate general high-dimensional nonlinear parabolic problems and cannot calculate higher-dimensional problems (e.g., more than 200 dimensions), and further the approximated error can also be reduced in terms of computational accuracy. These inspired us to carry out the following research.

The main contributions of this work are as follows: (i) we improve the method of Beck et al. [4] in order to further improve the accuracy of the solution. We apply multi-scale fusion technology [35, 39, 56] to the original neural network model, that is, use different scales to spatially discretize it, and finally use the merged results. This paper currently uses 4 scales for fusion, (ii) we also generalize the approach in [4] so that higher-dimensional models can be solved. The method of [4] is to spatially discretize the time-discrete data in the form of vectors. We first arrange the time-discrete data into a matrix and then use the convolutional neural networks [44, 55] for spatial discretizations. From the experimental results, the dimension of the solution is further expanded, and the time spent is also shorter. At present, we mainly enumerate numerical experiments in 256 and 400 dimensions, (iii) we mainly solve three practical high-dimensional examples, which possess the significant physical background, namely, the Allen-Cahn (AC), the Hamilton-Jacobi-Bellman (HJB), and the Black-Scholes-Barenblatt (BSB) equations. The numerical results can demonstrate the effectiveness of the

proposed approximation method and (iv) the proposed strategy considers advanced optimization algorithms, i.e., Adam optimizer and stochastic gradient descent-type optimization.

Following these ideas, the organizational structure of this work is as follows. Section 2 introduces merged construction of PDEs and 2BSDEs. Section 3 presents the forward temporal discretizations of the merged PDEs-2BSDEs system, spatial discretizations based on multiscale deep learning fusion and convolutional neural network, respectively, and corresponding optimization algorithms. Section 4 reports some experiments for numerical solutions of the merged PDEs-2BSDEs system, concretely, containing the high-dimensional AC, BSB and HJB equations. Finally, Section 5 summarizes the concluding remarks.

2. Merged PDEs-2BSDEs system

This section mainly intends to obtain a merged PDEs-2BSDEs system. First, we shall introduce the fully nonlinear second-order PDEs. Besides, Table 1 summarizes some notions and notations used in this paper.

Table 1: Summarization of notion and notations.

	Notion	Notation
Function symbol	The needed unkonwn function	$u(t,\mathbf{x})$(abbr. u)
	The boundary function of time	$\hat{g}(\mathbf{x})(u(T,\mathbf{x}) = \hat{g}(\mathbf{x}))$
	The function on the right side of the equation	$F\left(t,\mathbf{x},u(t,\mathbf{x}),(\nabla_{\mathbf{x}}u)(t,\mathbf{x}),(\mathrm{Hess}_{\mathbf{x}}u)(t,\mathbf{x})\right)$
Stochastic symbol	The probability space	$(\Omega,\mathcal{F},\mathbb{P})$
	The standard Brownian motion	$\mathcal{W}$
	The normal filtration generated via $\mathcal{W}$	$\mathbb{F}_t$(abbr. $\mathbb{F}$)
	The $\mathbb{F}$-adapted stochastic process	$\mathcal{X},\mathcal{Y},\mathcal{Z},\Gamma,\mathcal{A}$
	The state of the $\mathbb{F}$-adapted stochastic process at time t	$\mathcal{X}_t,\mathcal{Y}_t,\mathcal{Z}_t,\Gamma_t,\mathcal{A}_t$
Deep learning symbol	The approximate function by deep learning	$\mathbf{G}_n^\theta,\mathbf{A}_n^\theta,\mathcal{Y}_n^\theta,\mathcal{Z}_n^\theta,\tilde{\mathbf{G}}_n^\theta,\tilde{\mathbf{A}}_n^\theta$
	The activation function(ReLU function)	$\mathbf{R}_k(\mathbf{x})$
	The linear affine function	$\mathbf{M}_{k,l}^{\theta,v}$
	The d_i scale neural networks	$\mathbf{G}_{d_i}^\theta,\mathbf{A}_{d_i}^\theta$
	The convolution function	$\mathbf{M}_{k,l}^{\theta,v}$
	The i channel convolution neural networks	$\tilde{\mathbf{G}}_i^\theta,\tilde{\mathbf{A}}_i^\theta$
	The loss function of training	$\tilde{\phi}^{m,\mathbf{s}}(\theta,\omega)$
	The function of learning rate	$\tilde{\gamma}(m)$(abbr. $\tilde{\gamma}_m$)
Basic symbol	The dimension of $\mathbf{x}$	$d(d\in\mathbb{Z}^+)$
	The range of t	$T(0<T<\infty)$
	The number of time discrete points	$N(N\geq 1)$
	The certain point in time	$t_n(0\leq n\leq N-1)$
	The number of parameters in deep learning	v
	The number of channels in convolution neural network	$c(c\geq 1)$

2.1. Fully nonlinear second-order PDEs

Let $d\in\mathbb{Z}^+$, $0<T<\infty$, $u=(u(t,\mathbf{x}))_{0\leq t\leq T,\mathbf{x}\in\mathbb{R}^d}\in C^{1,3}\left([0,T]\times\mathbb{R}^d,\mathbb{R}\right)$, $F\in C([0,T]\times\mathbb{R}^d\times\mathbb{R}\times\mathbb{R}^d\times\mathbb{R}^{d\times d},\mathbb{R})$ and $\hat{g}\in C(\mathbb{R}^d,\mathbb{R})$ satisfy that $u(T,\mathbf{x})=\hat{g}(\mathbf{x})$ and

$$\frac{\partial u}{\partial t}(t,\mathbf{x})=F\left(t,\mathbf{x},u(t,\mathbf{x}),(\nabla_{\mathbf{x}}u)(t,\mathbf{x}),(\mathrm{Hess}_{\mathbf{x}}u)(t,\mathbf{x})\right), \tag{1}$$

for all $t\in[0,T)$ and $\mathbf{x}\in\mathbb{R}^d$.

Then, the deep-learning 2BSDE approaches can effective approximate the function $u(0,\mathbf{x})\in\mathbb{R}$ with $\mathbf{x}\in\mathbb{R}^d$. Note that deep-learning 2BSDE techniques can be easily extended to the case of fully nonlinear

3

second-order parabolic PDEs, but for keeping the symbolic complexity as low as possible, we restrict ourselves to the scalar case in this work (see (1)).

Furthermore, equation (1) is formulated as a terminal value problem. We select the terminal value problem instead of the initial value problem, which is more common in the literature of PDEs. On the one hand, the terminal value problem seems to be more naturally associated with 2BSDEs (see Section 2.2), and on the other hand, the terminal value problem naturally appears in financial engineering applications such as the BSB equation in derivatives pricing (see Section 4.2). Obviously, terminal value problems can be transformed into initial value problems and vice versa, which can be seen in the following Lemma.

Lemma 1. [4, Lemma 3.1] Let $d \in \mathbb{Z}^+$, $0 < T < \infty$, $F : [0, T] \times \mathbb{R}^d \times \mathbb{R} \times \mathbb{R}^d \times \mathbb{R}^{d \times d} \to \mathbb{R}$ and $\hat{g} : \mathbb{R}^d \to \mathbb{R}$, and assume that $u : [0, T] \times \mathbb{R}^d \to \mathbb{R}$ be a continuous function such that $u(T, \mathbf{x}) = \hat{g}(\mathbf{x}), u|_{[0,T) \times \mathbb{R}^d} \in C^{1,2}\left([0, T) \times \mathbb{R}^d, \mathbb{R}\right)$ and

$$\frac{\partial u}{\partial t}(t, \mathbf{x}) = F\left(t, \mathbf{x}, u(t, \mathbf{x}), (\nabla_{\mathbf{x}} u)(t, \mathbf{x}), (\mathrm{Hess}_{\mathbf{x}} u)(t, \mathbf{x})\right), \tag{2}$$

for all $(t, \mathbf{x}) \in [0, T) \times \mathbb{R}^d$. Assume $\widehat{F} : [0, T] \times \mathbb{R}^d \times \mathbb{R} \times \mathbb{R}^d \times \mathbb{R}^{d \times d} \to \mathbb{R}$ and $V : [0, T] \times \mathbb{R}^d \to \mathbb{R}$ be the functions such that $V(t, \mathbf{x}) = u(T - t, \mathbf{x})$ and

$$\widehat{F}(t, \mathbf{x}, \mathbf{y}, \mathbf{z}, \rho) = -F(T - t, \mathbf{x}, \mathbf{y}, \mathbf{z}, \rho), \tag{3}$$

for all $(t, \mathbf{x}, \mathbf{y}, \mathbf{z}, \rho) \in [0, T] \times \mathbb{R}^d \times \mathbb{R} \times \mathbb{R}^d \times \mathbb{R}^{d \times d}$. Then we get that $V : [0, T] \times \mathbb{R}^d \to \mathbb{R}$ is a continuous function, such that $V(0, x) = \hat{g}(x), V|_{(0,T] \times \mathbb{R}^d} \in C^{1,3}\left((0, T] \times \mathbb{R}^d, \mathbb{R}\right)$ and

$$\frac{\partial V}{\partial t}(t, \mathbf{x}) = \widehat{F}\left(t, \mathbf{x}, V(t, \mathbf{x}), (\nabla_{\mathbf{x}} V)(t, \mathbf{x}), (\mathrm{Hess}_{\mathbf{x}} V)(t, \mathbf{x})\right), \tag{4}$$

for all $(t, \mathbf{x}) \in (0, T] \times \mathbb{R}^d$.

Based on the above discussion, in the following numerical examples, we only consider the terminal problem.

2.2. Combination between fully nonlinear second-order PDEs and 2BSDEs

We apply the deep-learning 2BSDE approaches depend on a combination between fully nonlinear second-order PDEs and 2BSDEs (see the following Lemma 2), from which, Itô' lemma and some suitable assumptions are employed (see [4]).

Lemma 2. [4, Lemma 3.1] Assume that $d \in \mathbb{Z}^+$, $0 < T < \infty$, and that $u = (u(t, \mathbf{x}))_{t \in [0,T], \mathbf{x} \in \mathbb{R}^d} \in C^{1,3}\left([0, T] \times \mathbb{R}^d, \mathbb{R}\right), \mu \in C\left(\mathbb{R}^d, \mathbb{R}^d\right), \sigma \in C\left(\mathbb{R}^d, \mathbb{R}^{d \times d}\right), F : [0, T] \times \mathbb{R}^d \times \mathbb{R} \times \mathbb{R}^d \times \mathbb{R}^{d \times d} \to \mathbb{R}$, and $\hat{g} : \mathbb{R}^d \to \mathbb{R}$ be functions such that $\nabla_{\mathbf{x}} u \in C^{1,2}\left([0, T] \times \mathbb{R}^d, \mathbb{R}^d\right), u(T, \mathbf{x}) = \hat{g}(\mathbf{x})$ and

$$\frac{\partial u}{\partial t}(t, \mathbf{x}) = F\left(t, \mathbf{x}, u(t, \mathbf{x}), (\nabla_{\mathbf{x}} u)(t, \mathbf{x}), (\mathrm{Hess}_{\mathbf{x}} u)(t, \mathbf{x})\right), \tag{5}$$

for all $t \in [0, T)$ and $\mathbf{x} \in \mathbb{R}^d$. Then, assume that $(\Omega, \mathcal{F}, \mathbb{P})$ is a probability space, that $\mathcal{W} = \left(\mathcal{W}^{(1)}, \ldots, \mathcal{W}^{(d)}\right) : [0, T] \times \Omega \to \mathbb{R}^d$ is a standard Brownian motion on $(\Omega, \mathcal{F}, \mathbb{P})$, that $\mathbb{F} = (\mathbb{F}_t)_{t \in [0,T]}$ is the normal filtration on $(\Omega, \mathcal{F}, \mathbb{P})$ generated via $\mathcal{W}$, that $\xi : \Omega \to \mathbb{R}^d$ is a $\mathcal{F}_0/\mathcal{B}\left(\mathbb{R}^d\right)$-measurable function, and that $\mathcal{X} = \left(\mathcal{X}^{(1)}, \ldots, \mathcal{X}^{(d)}\right) : [0, T] \times \Omega \to \mathbb{R}^d$ is an $\mathbb{F}$-adapted stochastic process, with continuous sample paths such that for all $0 \leq t \leq T$, it holds $\mathbb{P}$-a.s. that

$$\mathcal{X}_t = \xi + \int_0^t \mu\left(\mathcal{X}_s\right) \mathrm{d}s + \int_0^t \sigma\left(\mathcal{X}_s\right) \mathrm{d}\mathcal{W}_s, \tag{6}$$

for all $\varpi \in C^{1,3}\left([0, T] \times \mathbb{R}^d, \mathbb{R}\right)$, and let $\mathcal{L}\varpi : [0, T] \times \mathbb{R}^d \to \mathbb{R}$ be the function such that

$$(\mathcal{L}\varpi)(t, \mathbf{x}) = \left(\frac{\partial \varpi}{\partial t}\right)(t, \mathbf{x}) + \frac{1}{2}\mathrm{Trace}\left(\sigma(\mathbf{x})\sigma(\mathbf{x})^*(\mathrm{Hess}_{\mathbf{x}} \varpi)(t, \mathbf{x})\right), \tag{7}$$

4

for all $(t, \mathbf{x}) \in [0, T] \times \mathbb{R}^d$, and let $\mathcal{Y} : [0, T] \times \Omega \rightarrow \mathbb{R}$, $\mathcal{Z} = \left(\mathcal{Z}^{(1)}, \ldots, \mathcal{Z}^{(d)} \right) : [0, T] \times \Omega \rightarrow \mathbb{R}^d$, $\Gamma = \left(\Gamma^{(i,j)} \right)_{(i,j) \in \{1, \ldots, d\}^2} : [0, T] \times \Omega \rightarrow \mathbb{R}^{d \times d}$, and let $\mathcal{A} = \left(\mathcal{A}^{(1)}, \ldots, \mathcal{A}^{(d)} \right) : [0, T] \times \Omega \rightarrow \mathbb{R}^d$ be the stochastic processes, such that

$$\mathcal{Y}_t = u(t, \mathcal{X}_t), \;\; \mathcal{Z}_t = (\nabla_x u)(t, X_t), \;\; \Gamma_t = (\text{Hess}_{\mathbf{x}}\, u)(t, \mathcal{X}_t), \;\; \mathcal{A}_t^{(i)} = \left(\mathcal{L} \left(\frac{\partial u}{\partial \mathbf{x}_i} \right) \right)(t, \mathcal{X}_t) \tag{8}$$

for all $0 \leq t \leq T$ and $i \in \{1, 2, \ldots, d\}$. Then, we obtain that $\mathcal{Y}, \mathcal{Z}, \Gamma, \mathcal{A}$ are $\mathbb{F}$-adapted stochastic processes, with continuous sample paths which satisfy that for all $0 \leq t \leq T$, it holds $\mathbb{P}$-a.s. that

$$\mathcal{Y}_t = \hat{g}(\mathcal{X}_T) - \int_t^T \left(F(s, \mathcal{X}_s, \mathcal{Y}_s, \mathcal{Z}_s, \Gamma_s) + \frac{1}{2} \text{Trace} \left(\sigma(\mathcal{X}_s) \sigma(\mathcal{X}_s)^* \Gamma_s \right) \right) ds$$
$$- \int_t^T \langle \mathcal{Z}_s, d\mathcal{X}_s \rangle_{\mathbb{R}^d} \tag{9}$$

and

$$\mathcal{Z}_t = \mathcal{Z}_0 + \int_0^t \mathcal{A}_s ds + \int_0^t \Gamma_s d\mathcal{X}_s. \tag{10}$$

2.3. Merged construction of PDEs and 2BSDEs

In what follows, we present a merged construction for PDE (1) and 2BSDE system. Let the hypotheses in Lemma 2 be satisfied and use the same notations as Lemma 2. Then, one can easily see that for $0 \leq \delta_1, \delta_2 \leq T$,

$$\mathcal{X}_{\delta_2} = \mathcal{X}_{\delta_1} + \int_{\delta_1}^{\delta_2} \mu(\mathcal{X}_s) ds + \int_{\delta_1}^{\delta_2} \sigma(\mathcal{X}_s) d\mathcal{W}_s, \tag{11}$$

$$\mathcal{Y}_{\delta_2} = \mathcal{Y}_{\delta_1} + \int_{\delta_1}^{\delta_2} \langle \mathcal{Z}_s, d\mathcal{X}_s \rangle_{\mathbb{R}^d}$$
$$+ \int_{\delta_1}^{\delta_2} \left(F(s, \mathcal{X}_s, \mathcal{Y}_s, \mathcal{Z}_s, (\text{Hess}_{\mathbf{x}}\, u)(s, \mathcal{X}_s)) + \frac{1}{2} \text{Trace} \left(\sigma(\mathcal{X}_s) \sigma(\mathcal{X}_s)^* (\text{Hess}_{\mathbf{x}}\, u)(s, \mathcal{X}_s) \right) \right) ds \tag{12}$$

and

$$\mathcal{Z}_{\delta_2} = \mathcal{Z}_{\delta_1} + \int_{\delta_1}^{\delta_2} (\mathcal{L}(\nabla_{\mathbf{x}} u))(s, \mathcal{X}_s) ds + \int_{\delta_1}^{\delta_2} (\text{Hess}_{\mathbf{x}}\, u)(s, \mathcal{X}_s) d\mathcal{X}_s. \tag{13}$$

3. Approximation of the merged PDEs-2BSDEs system

3.1. Forward-discretizations of the merged PDEs-2BSDEs system

Now, we describe a forward discretization of the merged PDEs-2BSDEs system (11)-(13). Let us consider positive integer $N \geq 1$ with $t_0, t_1, \ldots, t_N \in [0, T]$, such that

$$0 = t_0 < t_1 < t_2 < \ldots < t_N = T,$$

from which, the max mesh size $\tau := \max_{0 \leq j \leq N-1} (t_{j+1} - t_j)$ is sufficiently small and we define $\tau_j = t_j - t_{j-1}$ for $1 \leq j \leq N$.

Notice that, for sufficiently large $N \in \mathbb{Z}^+$, (6)-(8) and (11)-(13) indicate that for all $n \in \{0, 1, \ldots, N-1\}$, it holds that

$$\mathcal{X}_{t_0} = \mathcal{X}_0 = \xi, \qquad \mathcal{Y}_{t_0} = \mathcal{Y}_0 = u(0, \xi), \qquad \mathcal{Z}_{t_0} = \mathcal{Z}_0 = (\nabla_{\mathbf{x}} u)(0, \xi), \tag{14}$$

5

$$\mathcal{X}_{t_{n+1}} \approx \mathcal{X}_{t_n} + \mu\left(\mathcal{X}_{t_n}\right)\tau_{n+1} + \sigma\left(\mathcal{X}_{t_n}\right)\left(\mathcal{X}_{t_{n+1}} - \mathcal{X}_{t_n}\right), \tag{15}$$

$$
\begin{aligned}
\mathcal{Y}_{t_{n+1}} \approx \mathcal{Y}_{t_n} + &\Big[F\big(t_n, \mathcal{X}_{t_n}, \mathcal{Y}_{t_n}, \mathcal{Z}_{t_n}, (\mathrm{Hess}_{\mathbf{x}}\, u)(t_n, \mathcal{X}_{t_n})\big) \\
&+ \frac{1}{2}\,\mathrm{Trace}(\sigma(\mathcal{X}_{t_n})\sigma(\mathcal{X}_{t_n})^*(\mathrm{Hess}_{\mathbf{x}}\, u)(t_n, \mathcal{X}_{t_n}))\Big]\tau_{n+1} + \langle \mathcal{Z}_{t_n}, \mathcal{X}_{t_{n+1}} - \mathcal{X}_{t_n}\rangle_{\mathbb{R}^d},
\end{aligned}
\tag{16}
$$

and

$$\mathcal{Z}_{t_{n+1}} \approx \mathcal{Z}_{t_n} + \left(\mathcal{L}\left(\nabla_{\mathbf{x}} u\right)\right)(t_n, \mathcal{X}_{t_n})\tau_{n+1} + (\mathrm{Hess}_{\mathbf{x}}\, u)\left(t_n, \mathcal{X}_{t_n}\right)\left(\mathcal{X}_{t_{n+1}} - \mathcal{X}_{t_n}\right). \tag{17}$$

Naturally, we can obtain the semi-discretization approximation of the merged PDEs-2BSDEs system by (14)-(17).

3.2. Spatial discretizations based on multiscale deep learning fusion

In the following, for all $0 \le n \le N-1$ and $\mathbf{x} \in \mathbb{R}^d$, we select suitable approximations for functions $(\mathrm{Hess}_{\mathbf{x}}\, u)(t_n, \mathbf{x}) \in \mathbb{R}^{d\times d}$ and $(\mathcal{L}(\nabla_{\mathbf{x}} u))(t_n, \mathbf{x}) \in \mathbb{R}^d$ given in (16)-(17) and for the functions $u(t_n, \mathbf{x}) \in \mathbb{R}^d$ and $(\nabla_{\mathbf{x}} u)(t_n, \mathbf{x}) \in \mathbb{R}^d$. Precisely, we assume that $\nu \in \mathbb{N} \cap [d+1, \infty)$ for every $\theta \in \mathbb{R}^\nu, 0 \le n \le N$.

Assume $\mathbf{G}_n^\theta : \mathbb{R}^d \to \mathbb{R}^{d\times d}$ and $\mathbf{A}_n^\theta : \mathbb{R}^d \to \mathbb{R}^d$ are continuous functions, and then, for every $\theta = (\theta_1, \theta_2, \ldots, \theta_\nu) \in \mathbb{R}^\nu$, assume $\mathcal{Y}^\theta : \{0, 1, \ldots, N\} \times \Omega \to \mathbb{R}$ and $\mathcal{Z}^\theta : \{0, 1, \ldots, N\} \times \Omega \to \mathbb{R}^d$ be stochastic processes, such that $\mathcal{Y}_0^\theta = \theta_1$, $\mathcal{Z}_0^\theta = (\theta_2, \theta_3, \ldots, \theta_{d+1})$,

$$
\begin{aligned}
\mathcal{Y}_{n+1}^\theta = \mathcal{Y}_n^\theta + &\left\langle \mathcal{Z}_n^\theta, \mathcal{X}_{t_{n+1}} - \mathcal{X}_{t_n}\right\rangle_{\mathbb{R}^d} \\
&+ \left(F\left(t_n, \mathcal{X}_n, \mathcal{Y}_n^\theta, \mathcal{Z}_n^\theta, \mathbf{G}_n^\theta\left(\mathcal{X}_n\right)\right) + \frac{1}{2}\,\mathrm{Trace}\left(\mathbf{G}_n^\theta\left(\mathcal{X}_n\right)\right)\right)\tau_{n+1}
\end{aligned}
\tag{18}
$$

and

$$\mathcal{Z}_{n+1}^\theta = \mathcal{Z}_n^\theta + \mathbf{A}_n^\theta\left(\mathcal{X}_n\right)\tau_{n+1} + \mathbf{G}_n^\theta\left(\mathcal{X}_n\right)\left(\mathcal{X}_{t_{n+1}} - \mathcal{X}_{t_n}\right), \tag{19}$$

for $0 \le n \le N-1$. For all favorable $\theta \in \mathbb{R}^\nu, \mathbf{x} \in \mathbb{R}^d$ and $0 \le n \le N-1$, we select the suitable approximations that $\mathcal{Y}_n^\theta \approx \mathcal{Y}_{t_n}$, $\mathcal{Z}_n^\theta \approx \mathcal{Z}_{t_n}$, $\mathbf{G}_n^\theta(\mathbf{x}) \approx (\mathrm{Hess}_{\mathbf{x}} u)(t_n, \mathbf{x})$ and $\mathbf{A}_n^\theta(\mathbf{x}) \approx (\mathcal{L}(\nabla_{\mathbf{x}} u))(t_n, \mathbf{x})$.

Especially, we regard θ_1 and $(\theta_2, \theta_3, \ldots, \theta_{d+1})$ as the suitable approximations of $u(0, \xi)$ and $(\nabla_{\mathbf{x}} u)(0, \xi)$ with $u(0, \xi) \in \mathbb{R}$ and $(\nabla_{\mathbf{x}} u)(0, \xi) \in \mathbb{R}^d$. Then we can select the functions $\mathbf{G}_{d_i}^\theta$ and $\mathbf{A}_{d_i}^\theta$ as deep neural networks. In particular, d_i represents the scale of different neural networks, and four scales are selected here. Furthermore, we use the same neural network for different time n. That is, the parameters of our network only depend on different scales, independent of time n.

Assume $\nu \ge \left(2\sum_{i=1}^4 d_i + d + 1\right)(d+1) + \sum_{i=1}^4 (2d_i + d^2 + d)(d_i + 1)$. Supposing for all $\theta = (\theta_1, \ldots, \theta_\nu) \in \mathbb{R}^\nu, \mathbf{x} \in \mathbb{R}^d$, we have

$$\mathbf{G}_0^\theta(\mathbf{x}) = \begin{pmatrix} \theta_{d+2} & \theta_{d+3} & \ldots & \theta_{2d+1} \\ \theta_{2d+2} & \theta_{2d+3} & \ldots & \theta_{3d+1} \\ \vdots & \vdots & \vdots & \vdots \\ \theta_{d^2+2} & \theta_{d^3+3} & \ldots & \theta_{d^2+d+1} \end{pmatrix} \in \mathbb{R}^{d\times d} \text{ and } \mathbf{A}_0^\theta(\mathbf{x}) = \begin{pmatrix} \theta_{d^2+d+2} \\ \theta_{d^2+d+3} \\ \vdots \\ \theta_{d^2+2d+1} \end{pmatrix} \in \mathbb{R}^d.$$

With all $k \in \mathbb{N}$, we let $\mathbf{R}_k : \mathbb{R}^k \to \mathbb{R}^k$ be the activation function (ReLU), such that

$$\mathbf{R}_k(\mathbf{x}) = \Big(\max\{\mathbf{x}_1, 0\}, \ldots, \max\{\mathbf{x}_k, 0\}\Big), \tag{20}$$

for every $\mathbf{x} = (\mathbf{x}_1, \ldots, \mathbf{x}_k) \in \mathbb{R}^k$. For every $\theta = (\theta_1, \ldots, \theta_\nu) \in \mathbb{R}^\nu$, $v \in \mathbb{N}_0$, $k, l \in \mathbb{N}$ and $v + k(l+1) \leq \nu$, assume $\mathbf{M}_{k,l}^{\theta,v} : \mathbb{R}^l \to \mathbb{R}^k$ is the affine linear function, such that

$$\mathbf{M}_{k,l}^{\theta,v}(\mathbf{x}) = \begin{pmatrix} \theta_{v+1} & \theta_{v+2} & \cdots & \theta_{v+l} \\ \theta_{v+l+1} & \theta_{v+l+2} & \cdots & \theta_{v+2l} \\ \theta_{v+2l+1} & \theta_{v+2l+2} & \cdots & \theta_{v+3l} \\ \vdots & \vdots & \vdots & \vdots \\ \theta_{v+(k-1)l+1} & \theta_{v+(k-1)l+2} & \cdots & \theta_{v+kl} \end{pmatrix} \begin{pmatrix} \mathbf{x}_1 \\ \mathbf{x}_2 \\ \mathbf{x}_3 \\ \vdots \\ \mathbf{x}_l \end{pmatrix} + \begin{pmatrix} \theta_{v+kl+1} \\ \theta_{v+kl+2} \\ \theta_{v+kl+3} \\ \vdots \\ \theta_{v+kl+k} \end{pmatrix} := \mathbf{P}\mathbf{x}^T + \mathbf{Q}, \quad (21)$$

for all $\mathbf{x} = (\mathbf{x}_1, \ldots, \mathbf{x}_l)$. For every $\theta \in \mathbb{R}^\nu$, $\{d_i | i \in \{1, 2, 3, 4\}, d_0 = 0\}$, $d^t = \sum_{i=1}^4 d_i$, $d^{t^2} = \sum_{i=1}^4 d_i^2 + d_i$, $d^{t^3} = \sum_{i=1}^4 (d_i + d)(d_i + 1)$ and $\mathbf{x} \in \mathbb{R}^d$, we assume that

$$\begin{aligned} \mathbf{A}_{d_i}^\theta &= \mathbf{M}_{d,d_i}^{\theta,(d^t+d+1)(d+1)+d^{t^2}+\sum_1^{i-1} d(d_i+1)} \circ \mathbf{R}_{d_i} \circ \\ &\quad \mathbf{M}_{d_i,d_i}^{\theta,(d^t+d+1)(d+1)+\sum_1^{i-1} d_i^2+d_i} \circ \mathbf{R}_{d_i} \circ \mathbf{M}_{d_i,d}^{\theta,(\sum_1^{i-1} d_i+d+1)(d+1)}, \end{aligned} \quad (22)$$

and that

$$\begin{aligned} \mathbf{G}_{d_i}^\theta &= \mathbf{M}_{d^2,d_i}^{\theta,(2d^t+d+1)(d+1)+d^{t^3}+d^{t^2}+\sum_1^{i-1} d^2(d_i+1)} \circ \mathbf{R}_{d_i} \circ \\ &\quad \mathbf{M}_{d_i,d_i}^{\theta,(2d^t+d+1)(d+1)+d^{t^3}+\sum_1^{i-1} d_i^2+d_i} \circ \mathbf{R}_{d_i} \circ \mathbf{M}_{d_i,d}^{\theta,(\sum_1^{i-1} d_i+d^t+d+1)(d+1)+d^{t^3}}. \end{aligned} \quad (23)$$

Remark 1. In this remark, we illustrate the multiscale deep learning fusion and the specific choice of the $\nu \in \mathbb{N}$ in the above.

(i) Multiscale fusion is mainly reflected in function $\mathbf{A}_{d_i}^\theta$ and $\mathbf{G}_{d_i}^\theta$. We use deep neural networks of different scales to obtain $\mathbf{A}_{d_i}^\theta$ and $\mathbf{G}_{d_i}^\theta$, then fuse them to get the final result. In fact, multiscale fusion is to obtain more information in neural network training, thereby improving training results. In addition, if it is assumed that the scales selected each time are the same, then our multiscale fusion is equivalent to a weighted average of multiple experiments. From a probabilistic point of view, the results of multiple experiments are often more accurate and stable than the results of a single experiment.

(ii) For the specific choice of the ν, the choice of ν is mainly divided into three parts. On the one hand, it is employed to approximate the variables we need, which includes the real number $u(0, \xi) \in \mathbb{R}$, the $(1 \times d)$ matrix $(\nabla_{\mathbf{x}} u)(0, \xi)$, the $(d \times d)$ matrix $\mathbf{G}_0^\theta$ and $(d \times 1)$ vector $\mathbf{A}_0^\theta$. So, we have $\nu \geq (d+1)(d+1)$. On the other hand, the remaining two parts are related to neural networks, the first part is about $\mathbf{A}_{d_i}^\theta$, and the last part is about $\mathbf{G}_{d_i}^\theta$.

(iii) For the $\mathbf{A}_{d_i}^\theta$, in each of the employed d_i neural network we use $d_i(d+1)$ components of θ to describe the affine linear function from the d-dimensional first layer (input layer) to the d_i-dimensional second layer (includes a $d_i \times d$ matrix and a d_i vector, see (21)). Next, we use $d_i(d_i + 1)$ to describe the d_i-dimensional second layer to the d_i-dimensional third layer. Finally, the $d(d_i + 1)$ is used in the d_i-dimensional third layer to the d_i-dimensional fourth layer (output layer). For the $\mathbf{G}_{d_i}^\theta$, the few layers are basically the same as $\mathbf{A}_{d_i}^\theta$, the only difference is that the $d^2(d_i + 1)$ is used in the d_i-dimensional third layer to the d_i-dimensional fourth layer. Therefore, combining the above analysis, we have

$$\begin{aligned} \nu &\geq (d+1)(d+1) + 2\sum_{i=1}^4 d_i(d+1) + 2\sum_{i=1}^4 d_i(d_i+1) + \sum_{i=1}^4 d(d_i+1) + \sum_{i=1}^4 d^2(d_i+1) \\ &= (2\sum_{i=1}^4 d_i + d + 1)(d+1) + \sum_{i=1}^4 (2d_i + d^2 + d)(d_i+1). \end{aligned}$$

(iv) We also depict the sketch of the architecture of multiscale deep learning fusion, see Figure 1. In Figure 1, when $t = t_0$, we first give the initial values $\mathcal{X}_{t_0}, (\mathcal{L}(\nabla_x u)(t_0, \mathcal{X}_{t_0}), (\text{Hess}_x u)(t_0, \mathcal{X}_{t_0})$. Then use the

7

initial value to calculate the variables of $t = t_i$ in turn $(1 \geq i \geq N-1)$, which $h_{d_i}^H$ represents the H layer of the neural network at the d_i scale. As can be seen from the figure, each $\mathcal{X}_{t_i}$ is trained by neural networks of four scales, and finally fused to obtain h^{fusion}. Note that for each time $t = t_i$, we use the same neural network, which is continuously updated as time changes. In addition, $(\mathcal{L}(\nabla_{\mathbf{x}} u))(t_i, \mathcal{X}_{t_i})$ and $(\text{Hess}_{\mathbf{x}} u)(t_i, \mathcal{X}_{t_i})$ are approximated separately using two networks. In Figure 1, it is not subdivided for the sake of brevity.
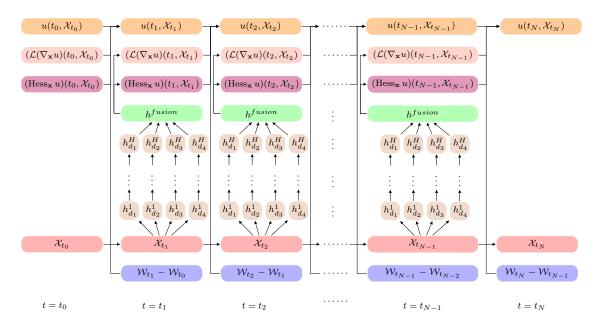

Figure 1: Sketch of the architecture of the multiscale deep learning fusion for BSDE.

3.3. Spatial discretizations based on convolutional neural network

Here, with $0 \leq n \leq N-1$ and $\mathbf{x} \in \mathbb{R}^d$, based on convolutional neural network, we still choose the suitable approximations for functions $(\text{Hess}_{\mathbf{x}} u)(t_n, \mathbf{x}) \in \mathbb{R}^{d \times d}$, $(\mathcal{L}(\nabla_{\mathbf{x}} u))(t_n, \mathbf{x}) \in \mathbb{R}^d$, $u(t_n, \mathbf{x}) \in \mathbb{R}^d$ and $(\nabla_{\mathbf{x}} u)(t_n, \mathbf{x}) \in \mathbb{R}^d$. Then let $\nu \in \mathbb{N} \cap [d+1, \infty)$ and θ is assumed as Subsection 3.2 with $0 \leq n \leq N$.

Suppose that $\widetilde{\mathbf{G}}_n^\theta : \mathbb{R}^d \to \mathbb{R}^{d \times d}$ and $\widetilde{\mathbf{A}}_n^\theta : \mathbb{R}^d \to \mathbb{R}^d$ are continuous functions. For every $\theta = (\theta_1, \theta_2, \ldots, \theta_\nu) \in \mathbb{R}^\nu$, assume $\mathcal{Y}^\theta$ and $\mathcal{Z}^\theta$ be denoted as before, which satisfy $\mathcal{Y}_0^\theta = \theta_1$, $\mathcal{Z}_0^\theta = (\theta_2, \theta_3, \ldots, \theta_{d+1})$,

$$
\begin{aligned}
\mathcal{Y}_{n+1}^\theta = \mathcal{Y}_n^\theta &+ \left\langle \mathcal{Z}_n^\theta, \mathcal{X}_{t_{n+1}} - \mathcal{X}_{t_n} \right\rangle_{\mathbb{R}^d} \\
&+ \left(F\left(t_n, \mathcal{X}_n, \mathcal{Y}_n^\theta, \mathcal{Z}_n^\theta, \widetilde{\mathbf{G}}_n^\theta(\mathcal{X}_n)\right) + \frac{1}{2} \text{Trace}\left(\widetilde{\mathbf{G}}_n^\theta(\mathcal{X}_n)\right) \right) \tau_{n+1}
\end{aligned}
\tag{24}
$$

and that

$$
\mathcal{Z}_{n+1}^\theta = \mathcal{Z}_n^\theta + \widetilde{\mathbf{A}}_n^\theta(\mathcal{X}_n) \tau_{n+1} + \widetilde{\mathbf{G}}_n^\theta(\mathcal{X}_n)(\mathcal{X}_{t_{n+1}} - \mathcal{X}_{t_n}),
\tag{25}
$$

for $0 \leq n \leq N-1$. Then, we can choose suitable approximations that $\mathcal{Y}_n^\theta \approx \mathcal{Y}_{t_n}$, $\mathcal{Z}_n^\theta \approx \mathcal{Z}_{t_n}$, $\widetilde{\mathbf{G}}_n^\theta(\mathbf{x}) \approx (\text{Hess}_{\mathbf{x}} u)(t_n, \mathbf{x})$ and $\widetilde{\mathbf{A}}_n^\theta(\mathbf{x}) \approx (\mathcal{L}(\nabla_{\mathbf{x}} u))(t_n, \mathbf{x})$, in view of convolutional neural network. In addition, we consider θ_1 and $(\theta_2, \theta_3, \ldots, \theta_{d+1})$ as the affable approximations of $u(0, \xi)$ and $(\nabla_{\mathbf{x}} u)(0, \xi)$. Also, we can choose functions $\widetilde{\mathbf{G}}_n^\theta$ and $\widetilde{\mathbf{A}}_n^\theta$ as deep convolutional neural networks with $0 \leq n \leq N-1$.

Similarly, as in Subsection 3.2, we use the same neural network for $\widetilde{\mathbf{A}}_n^\theta, \widetilde{\mathbf{G}}_n^\theta, \forall n$. The difference is that we introduce the channel c of the convolution kernel. Therefore, we use the new notation $\widetilde{\mathbf{A}}_i^\theta, \widetilde{\mathbf{G}}_i^\theta, 1 \leq i \leq c, i \in \mathbb{N}$. Suppose $\nu \geq [(4c+4)d + d^2 + 1](d+1)$ and for every $\theta = (\theta_1, \ldots, \theta_\nu) \in \mathbb{R}^\nu, \mathbf{x} \in \mathbb{R}^d$, we yield that $\widetilde{\mathbf{G}}_0^\theta(\mathbf{x}) = \mathbf{G}_0^\theta(\mathbf{x})$ and $\widetilde{\mathbf{A}}_0^\theta(\mathbf{x}) = \mathbf{A}_0^\theta(\mathbf{x})$. Assume $k \in \mathbb{N}$, and we let the activation function (ReLU) $\mathbf{R}_k(\mathbf{x})$

8

be given in (20) for every $\mathbf{x} = (\mathbf{x}_1, \ldots, \mathbf{x}_k) \in \mathbb{R}^k$. For every $\theta = (\theta_1, \ldots, \theta_\nu) \in \mathbb{R}^\nu$, $v \in \mathbb{N}_0$, $k, l \in \mathbb{N}$ and $v + k(l+1) \leq \nu$, suppose that $\widetilde{\mathbf{M}}_{k,l}^{\theta,v} : \mathbb{R}^l \to \mathbb{R}^k$ satisfies that

$$\widetilde{\mathbf{M}}_{k,l}^{\theta,v}(\mathbf{Z}) = \mathbf{P} \otimes \mathbf{Z} + \mathbf{Q}, \tag{26}$$

where the notation $\otimes$ represents the convolution rule, the matrix

$$\mathbf{Z} = \begin{pmatrix} \mathbf{x}_1 & \mathbf{x}_{\sqrt{k}+1} & \cdots & \mathbf{x}_{k-\sqrt{k}+1} \\ \mathbf{x}_2 & \mathbf{x}_{\sqrt{k}+2} & \cdots & \mathbf{x}_{k-\sqrt{k}+2} \\ \mathbf{x}_3 & \mathbf{x}_{\sqrt{k}+3} & \cdots & \mathbf{x}_{k-\sqrt{k}+3} \\ \vdots & \vdots & \vdots & \vdots \\ \mathbf{x}_{\sqrt{k}} & \mathbf{x}_{2\sqrt{k}} & \cdots & \mathbf{x}_k \end{pmatrix},$$

and $\mathbf{P}$, $\mathbf{Q}$ are presented in (21).

For all $\theta \in \mathbb{R}^\nu$, $1 \leq i \leq c$ and $\mathbf{x} \in \mathbb{R}^d$, suppose that

$$\widetilde{\mathbf{A}}_i^\theta = \mathbf{M}_{d,d}^{\theta,[(2c+2)d+1](d+1)} \circ \mathbf{Re} \left(\mathbf{R}_d \circ \widetilde{\mathbf{M}}_{d,d}^{\theta,[(2c+1)d+1](d+1)} \circ \mathbf{R}_d \circ \widetilde{\mathbf{M}}_{d,d}^{\theta,[(c+i)d+1](d+1)} \circ \mathbf{R}_d \circ \widetilde{\mathbf{M}}_{d,d}^{\theta,(id+1)(d+1)} \right), \tag{27}$$

and that

$$\widetilde{\mathbf{G}}_i^\theta = \mathbf{M}_{d^2,d}^{\theta,[(4c+4)d+1](d+1)} \circ \mathbf{Re} \left(\widetilde{\mathbf{M}}_{d^2,d}^{\theta,[(4c+3)d+1](d+1)} \circ \mathbf{R}_d \circ \widetilde{\mathbf{M}}_{d,d}^{\theta,[(3c+2+i)d+1](d+1)} \circ \mathbf{R}_d \circ \widetilde{\mathbf{M}}_{d,d}^{\theta,[(2c+2+i)d+1](d+1)} \right), \tag{28}$$

in which $\mathbf{Re}(\cdot)$ denotes the operation to pull the matrix $\mathbf{Z}$ back into the vector $\mathbf{x}$.

Remark 2. In this remark, we describe some details in convolutional neural networks.

(i) We used three convolutional layers and one linear layer. In the convolution layer, we use a convolution kernel of 3×3, and the stride and padding are both set to 1 by default. Therefore, the matrix size does not change after each convolution. In the first two convolutional layers, we set the number of channels to 32, and in the last convolutional layer, set the number of channels to 1. For the linear layer, we first pull the output of the convolutional layer into vector, then employ the linear transformation in Subsection 3.1.

(ii) For the specific choice of the ν, the basic calculation idea is consistent with Subsection 3.1. In first stage, we have $\nu \geq (d+1)(d+1)$ as same as Subsection 3.1. In second stage, the first two convolutional layers are $2c \cdot d(d+1)$, the final convolutional layer is $1 \cdot d(d+1)$ and the linear layer is $d(d+1)$ for $\tilde{\mathbf{A}}^\theta$. In third stage, for $\tilde{\mathbf{G}}^\theta$, except that the linear layer is $d^2(d+1)$, the others are the same as $\tilde{\mathbf{A}}^\theta$. We give a specific calculation formula here. For more specific information, please refer to Subsection 3.1.

$$\begin{aligned} \nu &\geq (d+1)(d+1) + 2c \cdot d(d+1) + 2c \cdot d(d+1) + 2 \cdot d(d+1) + d(d+1) + d^2(d+1) \\ &= [(4c+4)d + d^2 + 1](d+1). \end{aligned}$$

(iii) Figure 2 depicts the rough schematic diagram of convolutional neural network. In fact, other processing processes are similar to Figure 1. For simplicity, we only draw the process of the convolutional neural network here. As seen in Figure 2, $\mathbf{x}$ has to undergo a "reshape" operation to become $\mathbf{Z}$ before it can be input into the network. As can be seen from the figure, $\mathbf{Z}$ is subjected to a "conv" operation to obtain matrix $\mathbf{H}^{conv1}$ of multiple channels. For brevity, only 4 channels are drawn on the graph, there should actually be 32 channels. Note that, in the last layer of convolution $\mathbf{H}^{final}$, we turn the multiple channels back into a single channel. In addition, the "reshape+FC" operation means that the matrix is first converted into vector by the "reshape" operation. Then "FC" is used to perform the operation. Here "FC" is the linear transformation in Subsection 3.2.
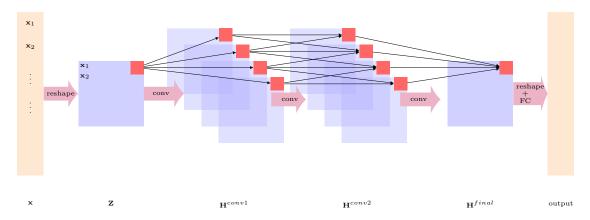
Figure 2: The rough schematic diagram of convolutional neural network.

3.4. Optimization algorithms

Here, we give the proposed optimization algorithms. First, we present the following lemma (see [4, Framework 3.2]).

Lemma 3. [4] Let $T, N, d, \varrho, \varsigma, \nu$ be defined as before. Let $F : [0,T] \times \mathbb{R}^d \times \mathbb{R} \times \mathbb{R}^d \times \mathbb{R}^{d \times d} \to \mathbb{R}$ and $\hat{g} : \mathbb{R}^d \to \mathbb{R}$ be functions, and $\left(\Omega, \mathcal{F}, \mathbb{P}, (\mathbb{F}_t)_{t \in [0,T]}\right)$ be defined as before. Assume for every $\theta \in \mathbb{R}^\nu$ let $\mathbb{U}^\theta : \mathbb{R}^d \to \mathbb{R}$ and $\mathbb{Z}^\theta : \mathbb{R}^d \to \mathbb{R}^d$ be functions and for every $m \in \mathbb{N}_0, j \in \mathbb{N}$ let $\mathcal{X}^{m,j} : \{0,1,\ldots,N\} \times \Omega \to \mathbb{R}^d$ be a stochastic process such that $\mathcal{X}_0^{m,j} = \xi^{m,j}$ and

$$\mathcal{X}_{n+1}^{m,j} = \mathcal{H}\left(t_n, t_{n+1}, \mathcal{X}_n^{m,j}, \mathcal{W}_{t_{n+1}}^{m,j} - \mathcal{W}_{t_n}^{m,j}\right),$$

for all $0 \leq n \leq N-1$. Then, for every $\theta \in \mathbb{R}^\nu, j \in \mathbb{N}, \mathbf{s} \in \mathbb{R}^\varsigma, n \in \{0,1,\ldots,N-1\}$, assume $\mathbb{G}_n^{\theta,j,\,\mathbf{s}} : \left(\mathbb{R}^d\right)^{\mathbb{N}_0} \to \mathbb{R}^{d \times d}$ and $\mathbb{A}_n^{\theta,j,\mathbf{s}} : \left(\mathbb{R}^d\right)^{\mathbb{N}_0} \to \mathbb{R}^d$ are functions. Besides, for every $\theta \in \mathbb{R}^\nu, m \in \mathbb{N}_0, j \in \mathbb{N}, \mathbf{s} \in \mathbb{R}^\varsigma$, we suppose that $\mathcal{Y}^{\theta,m,j,\,\mathbf{s}} : \{0,1,\ldots,N\} \times \Omega \to \mathbb{R}$ and $\mathcal{Z}^{\theta,m,j,\,\mathbf{s}} : \{0,1,\ldots,N\} \times \Omega \to \mathbb{R}^d$ be stochastic processes such that

$$\mathcal{Y}_0^{\theta,m,j,\mathbf{s}} = \mathbb{U}^\theta\left(\xi^{m,j}\right), \quad \mathcal{Z}_0^{\theta,m,j,\mathbf{s}} = \mathbb{Z}^\theta\left(\xi^{m,j}\right),$$

and

$$\begin{aligned}
\mathcal{Y}_{n+1}^{\theta,m,j,\mathbf{s}} = \mathcal{Y}_n^{\theta,m,j,\mathbf{s}} + \tau_{n+1}\bigg[&\frac{1}{2}\operatorname{Trace}(\sigma(\mathcal{X}_n^{m,j})\sigma(\mathcal{X}_n^{m,j})^* \mathbf{G}_n^{\theta,j,\mathbf{s}}((\mathcal{X}_n^{m,i})_{i \in \mathbb{N}})) \\
&+ F(t_n, \mathcal{X}_n^{m,j}, \mathcal{Y}_n^{\theta,m,j}, \mathcal{Z}_n^{\theta,m,j,\mathbf{s}}, \mathbf{G}_n^{\theta,j,\mathbf{s}}((\mathcal{X}_n^{m,i})_{i \in \mathbb{N}}))\bigg] + \langle \mathcal{Z}_n^{\theta,m,j,\mathbf{s}}, \mathcal{X}_{n+1}^{m,j} - \mathcal{X}_n^{m,j}\rangle_{\mathbb{R}^d}
\end{aligned}$$

and that

$$\mathcal{Z}_{n+1}^{\theta,m,j,\mathbf{s}} = \mathcal{Z}_n^{\theta,m,j,\mathbf{s}} + \mathbf{A}_n^{\theta,j,\mathbf{s}}\left(\left(\mathcal{X}_n^{m,i}\right)_{i \in \mathbb{N}}\right)\tau_{n+1} + \mathbf{G}_n^{\theta,j,\mathbf{s}}\left(\left(\mathcal{X}_n^{m,i}\right)_{i \in \mathbb{N}}\right)\left(\mathcal{X}_{n+1}^{m,j} - \mathcal{X}_n^{m,j}\right).$$

Assume $(\mathbf{J}_m)_{m \in \mathbb{N}_0} \subseteq \mathbb{N}$ is a sequence. For every $m \in \mathbb{N}_0, \mathbf{s} \in \mathbb{R}^\varsigma$, we let $\widetilde{\phi}^{m,\mathbf{s}} : \mathbb{R}^\nu \times \Omega \to \mathbb{R}$ be the function, such that

$$\widetilde{\phi}^{m,\mathbf{s}}(\theta,\omega) = \frac{1}{\mathbf{J}_m}\sum_{j=1}^{\mathbf{J}_m}\left|\mathcal{Y}_N^{\theta,m,j,\mathbf{s}}(\omega) - \hat{g}\left(\mathcal{X}_N^{m,j}(\omega)\right)\right|^2 \tag{29}$$

for all $(\theta,\omega) \in \mathbb{R}^\nu \times \Omega$. Then for every $m \in \mathbb{N}_0, \mathbf{s} \in \mathbb{R}^\varsigma$, suppose $\widetilde{\Phi}^{m,\,\mathbf{s}} : \mathbb{R}^\nu \times \Omega \to \mathbb{R}^\nu$ is a function which satisfies for all $\omega \in \Omega, \theta \in \left\{\zeta \in \mathbb{R}^\nu : \widetilde{\phi}^{m,\mathbf{s}}(\cdot,\omega) : \mathbb{R}^\nu \to \mathbb{R}\text{ is differentiable at }\zeta\right\}$ that

$$\widetilde{\Phi}^{m,\mathbf{s}}(\theta,\omega) = \left(\nabla_\theta\widetilde{\phi}^{m,\mathbf{s}}\right)(\theta,\omega),$$

10

and suppose that $\mathcal{S} : \mathbb{R}^{\varsigma} \times \mathbb{R}^{\nu} \times \left(\mathbb{R}^{d}\right)^{\{0,1,\dots,N-1\}\times\mathbb{N}} \to \mathbb{R}^{\varsigma}$ is a function, and for every $m \in \mathbb{N}_0$, we let $\widetilde{\psi}_m : \mathbb{R}^{\varrho} \to \mathbb{R}^{\nu}$ and $\widetilde{\Psi}_m : \mathbb{R}^{\varrho} \times \mathbb{R}^{\nu} \to \mathbb{R}^{\varrho}$ be functions. For all $m \in \mathbb{N}_0$, we let $\Theta : \mathbb{N}_0 \times \Omega \to \mathbb{R}^{\nu}$, $\mathbb{S} : \mathbb{N}_0 \times \Omega \to \mathbb{R}^{\varsigma}$, and $\widetilde{\Xi} : \mathbb{N}_0 \times \Omega \to \mathbb{R}^{\varrho}$ be stochastic processes, which satisfy that

$$\mathbb{S}_{m+1} = \mathcal{S}\left(\mathbb{S}_m, \Theta_m, \left(\mathcal{X}_n^{m,i}\right)_{(n,i)\in\{0,1,\dots,N-1\}\times\mathbb{N}}\right), \tag{30}$$

and that

$$\widetilde{\Xi}_{m+1} = \widetilde{\Psi}_m\left(\widetilde{\Xi}_m, \widetilde{\Phi}^{m,\mathbb{S}_{m+1}}\left(\Theta_m\right)\right), \qquad \Theta_{m+1} = \Theta_m - \widetilde{\psi}_m\left(\widetilde{\Xi}_{m+1}\right). \tag{31}$$

Below, we present several special choices for functions $\widetilde{\psi}_m, \widetilde{\Psi}_m, m \in \mathbb{N}$, given in (31). Based on that, we present the following optimization algorithms.

(i) **Stochastic gradient descent (SGD) method**. Provided the setting in Lemma 3, let notations $(\widetilde{\gamma}_m)_{m\in\mathbb{N}} \subseteq (0,\infty)$, and suppose for all $m \in \mathbb{N}, \mathbf{x} \in \mathbb{R}^{\varrho}, (\varphi_j)_{j\in\mathbb{N}} \in (\mathbb{R}^{\rho})^{\mathbb{N}}$ that

$$\varrho = \rho, \qquad \widetilde{\Psi}_m\left(\mathbf{x}, (\varphi_j)_{j\in\mathbb{N}}\right) = \varphi_1, \qquad \widetilde{\psi}_m(x) = \widetilde{\gamma}_m \mathbf{x},$$

and then it holds that

$$\Theta_m = \Theta_{m-1} - \widetilde{\gamma}_m \widetilde{\Phi}^{m-1}\left(\Theta_{m-1}\right),$$

for all $m \in \mathbb{N}$.

(ii) **Adaptive Moment Estimation (Adam) with mini-batches [37]**. Here, we use Adam optimizer with the deep-learning 2BSDE solver. Provided the setting in Lemma 3, suppose that $\varrho = 2\rho$, and assume $\mathrm{Pow}_{\hat{r}} : \mathbb{R}^{\rho} \to \mathbb{R}^{\rho}, 0 < \hat{r} < \infty$ is the functions satisfying that

$$\mathrm{Pow}_{\hat{r}}(x) = \left(|\mathbf{x}_1|^{\hat{r}}, \dots, |\mathbf{x}_{\rho}|^{\hat{r}}\right),$$

for all $0 < \hat{r} < \infty$ and $\mathbf{x} = (\mathbf{x}_1, \dots, \mathbf{x}_{\rho}) \in \mathbb{R}^{\rho}$.

Let $0 < \varepsilon < \infty, (\widetilde{\gamma}_m)_{m\in\mathbb{N}} \subseteq (0,\infty), (\mathbf{J}_m)_{m\in\mathbb{N}_0} \subseteq \mathbb{N}$ and $0 < \widehat{\mathbb{X}}, \widehat{\mathbb{Y}} < 1$, and assume that $\widehat{\mathbf{m}}, \widehat{\mathbb{M}} : \mathbb{N}_0 \times \Omega \to \mathbb{R}^{\rho}$ are the stochastic processes which satisfy for all $m \in \mathbb{N}_0$ that $\widetilde{\Xi}_m = \left(\widehat{\mathbf{m}}_m, \widehat{\mathbb{M}}_m\right)$, and suppose that

$$\widetilde{\Psi}_m\left(\mathbf{x}, \mathbf{y}, (\varphi_j)_{j\in\mathbb{N}}\right) = \left[\widehat{\mathbb{X}}\mathbf{x} + (1-\widehat{\mathbb{X}})\left(\frac{1}{\mathbf{J}_m}\sum_{j=1}^{\mathbf{J}_m}\varphi_j\right), \widehat{\mathbb{Y}}\mathbf{y} + (1-\widehat{\mathbb{Y}})\mathrm{Pow}_2\left(\frac{1}{\mathbf{J}_m}\sum_{j=1}^{\mathbf{J}_m}\varphi_j\right)\right]$$

and

$$\widetilde{\psi}_m(\mathbf{x}, \mathbf{y}) = \left[\varepsilon + \mathrm{Pow}_{\frac{1}{2}}(\mathbf{y})\right]^{-1}\widetilde{\gamma}_m\mathbf{x},$$

for all $m \in \mathbb{N}, \mathbf{x}, \mathbf{y} \in \mathbb{R}^{\rho}, (\varphi_j)_{j\in\mathbb{N}} \in (\mathbb{R}^{\rho})^{\mathbb{N}}$. Then for all $m \in \mathbb{N}$, we have

$$\widehat{\mathbb{M}}_m = \widehat{\mathbb{Y}}\widehat{\mathbb{M}}_{m-1} + (1-\widehat{\mathbb{Y}})\mathrm{Pow}_2\left(\frac{1}{\mathbf{J}_m}\sum_{j=1}^{\mathbf{J}_m}\widetilde{\Phi}_{\mathbb{S}_m}^{m-1,j}\left(\Theta_{m-1}\right)\right),$$

$$\widehat{\mathbf{m}}_m = \widehat{\mathbb{X}}\widehat{\mathbf{m}}_{m-1} + (1-\widehat{\mathbb{X}})\left(\frac{1}{\mathbf{J}_m}\sum_{j=1}^{\mathbf{J}_m}\widetilde{\Phi}_{\mathbb{S}_m}^{m-1,j}\left(\Theta_{m-1}\right)\right),$$

and the final update formula is

$$\Theta_m = \Theta_{m-1} - \left[\varepsilon + \mathrm{Pow}_{\frac{1}{2}}\left(\widehat{\mathbb{M}}_m\right)\right]^{-1}\widetilde{\gamma}_m\widehat{\mathbf{m}}_m.$$

Finally, we summarize the proposed approximation method in Algorithm 1.

Algorithm 1 Approximation algorithm using multi-scale deep learning fusion (or convolutional neural network).

Inputs: the functions $F(t, \mathbf{x}, u(t, \mathbf{x}), (\nabla_{\mathbf{x}} u)(t, \mathbf{x}), (\text{Hess}_{\mathbf{x}} u)(t, \mathbf{x}))$ and $\hat{g}(\mathbf{x})$.
Outputs: $u(0, \mathbf{x})$.
 1: Initialize $\mathcal{X}_{t_0}, \mathcal{Y}_{t_0}, \mathcal{Z}_{t_0}, \mathbf{G}, \mathbf{A}$.
 2: **for** $t = t_0 : t_N$ (each discrete time point) **do**
 3:     Updated the $\mathcal{X}_t, \mathcal{Y}_t$ by using (15) and (16).
 4:     Compute the $\mathbf{A}$ and $\mathbf{G}$ by using (22) and (23) (or (27) and (28)).
 5: **end for**
 6: **while** not up to total training steps **do**
 7:     Compute the loss function $\widetilde{\phi}^{m,\mathbf{s}}(\theta, \omega)$ by using (29).
 8:     Apply SGD or Adam algorithm to optimization the loss function $\widetilde{\phi}^{m,\mathbf{s}}(\theta, \omega)$.
 9:     Updated the neural networks (or convolutional neural network) paramters by back propagation.
10: **end while**
11: **if** the training is completed **then**
12:     Obtain the function value $\mathcal{Y}_{t_0}$.
13:     **return** $u(0, \mathbf{x}) = \mathcal{Y}_{t_0}$.
14: **end if**

---

4. Numerical results and discussion

This section employs the multiscale deep learning fusion and CNNs to approximately solve several stochastic PDEs, which mainly include the AC, HJB and BSB equations. Specifically, in Subsection 4.1, we first employ multiscale deep learning to solve the 20-dimensional AC equation and compare with the method of Beck et al. [4], and use the CNNs to obtain numerical solutions of the higher-dimensional AC equation. Then the numerical experiments in 256 and 400 dimensions are given, respectively. Subsections 4.2 and 4.3 also deal with the HJB and BSB equations, respectively, and the only difference is that when using multiscale deep learning method, we utilize the case 100 dimensions to replace that of 20 dimensions. All of the numerical experiments have been performed in Python 3.8 using TensorFlow 2.4, on NVIDIA Tesla P100 GPU (16GB memory). The simulation codes of proposed method are available on the GitHub page [1].

4.1. High-dimensional AC equation

This subsection discusses the approximate solution of the high-dimensional AC equation with a cubic nonlinearity (see (34)). Next, the following two examples show that the approximated calculation of Allen equations of different dimensions from multiscale deep learning fusion and convolutional neural networks, respectively.

Example 1. Multiscale deep learning fusion. Assuming the notations $T = \frac{3}{10}, \widetilde{\gamma} = \frac{1}{1000}, d = 20, \tilde{d} \in \{20, 30, 40, 50\}, N = 20, \xi = \{0, \ldots, 0\} \in \mathbb{R}^d, t \in [0, T), \mathbf{x}, \mathbf{z} \in \mathbb{R}^d, \mathbf{y} \in \mathbb{R}, S \in \mathbb{R}^{d \times d}, t_s = \frac{sT}{N}, \hat{g}(\mathbf{x}) = [2 + \frac{2}{5}||\mathbf{x}||_{\mathbb{R}^d}^2]^{-1}$, and

$$f(t, \mathbf{x}, \mathbf{y}, \mathbf{z}, S) = -\frac{1}{2}\text{Trace}(S) - \mathbf{y} + \mathbf{y}^3, \tag{32}$$

and suppose that $u : [0, T] \times \mathbb{R}^d \to \mathbb{R}$ is an at most polynomially growing continuous function, such that $u(T, \mathbf{x}) = \hat{g}(\mathbf{x}), u|_{[0,T) \times \mathbb{R}^d} \in C^{1,3}([0, T) \times \mathbb{R}^d, \mathbb{R})$, and

$$\frac{\partial u}{\partial t}(t, \mathbf{x}) = f(t, \mathbf{x}, u(t, \mathbf{x}), (\nabla_{\mathbf{x}} u)(t, \mathbf{x}), (\text{Hess}_{\mathbf{x}} u)(t, \mathbf{x})), \tag{33}$$

for all $(t, \mathbf{x}) \in [0, T] \times \mathbb{R}^d$. The solution $u : [0, T) \times \mathbb{R}^d \to \mathbb{R}$ of (33) such that $u(T, \mathbf{x}) = \left[2 + \frac{2}{5}||\mathbf{x}||_{\mathbb{R}^d}\right]^{-1}$ and

$$\frac{\partial u}{\partial t}(t, \mathbf{x}) + \frac{1}{2}(\triangle_{\mathbf{x}} u)(t, \mathbf{x}) + u(t, \mathbf{x}) - [u(t, \mathbf{x})]^3 = 0, \tag{34}$$
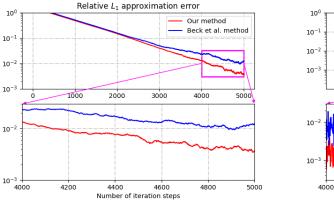
---

for all $(t, \mathbf{x}) \in [0, T] \times \mathbb{R}^d$.

Table 2 displays different methods to approximatively calculate the mean and standard deviation of u^{Θ_m} (i.e., $\mu_{u^{\Theta_m}}$ and $\sigma_{u^{\Theta_m}}$), the mean and standard deviation of corresponding L_1-approximation error associated to u^{Θ_m} (i.e., $\mu_{L^1_{\text{error}}}$ and $\sigma_{L^1_{\text{error}}}$), and the runtime in seconds needed to calculate one realization of u^{Θ_m} against $m \in \{0, 1000, 2000, 3000, 4000, 5000\}$ based on 10 independent runs. In addition, Figure 3 depicts approximations of the mean of the relative L_1-approximation error and approximations of the mean of the loss function associated to u^{Θ_m} against $m \in \{0, 1, 2, \ldots, 5000\}$ based on 10 independent realizations. In the approximative calculations of the relative L^1-approximation error, the value $u(0, \xi)$ of the solution u of the (34) has been replaced by the value 0.30879 which, in turn, has been calculated through the Branching diffusion method [25]. In particular, the relative L_1-approximation error is calculated as $\frac{|u^{\Theta_m} - 0.30879|}{0.30879}$.

It is not difficult to see from Table 2 that the approximate solution obtained by our method has higher accuracy, and the running time is also greatly reduced. To more intuitively compare with the existing methods, we draw Figure 3. Regarding the relative L^1-approximation error in Figure 3, proposed method is almost consistent with the method in [4] when the number of training steps is small. However, as the number of training steps increases, the proposed method has a smaller relative L^1-approximation error, which means that our method is more accurate and effective. In addition, we purposely magnify the relative L^1-approximation error from steps 4000 to 5000 to the lower part of the figure. From the enlarged picture, it can be clearly seen that our relative L^1-approximation error is already less than 0.01. At the same time, the right side of Figure 3 shows the trend of the loss function. As shown, our loss function value is smaller.

Table 2: Numerical simulations of the 20-dimensional AC equation.

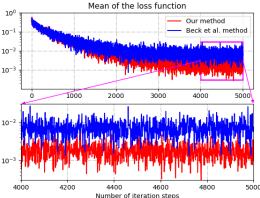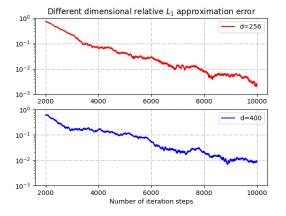| Method	Training steps	$\mu_{u^{\Theta_m}}$	$\sigma_{u^{\Theta_m}}$	$\mu_{L^1_{\text{error}}}$	$\sigma_{L^1_{\text{error}}}$	Mean of the loss function	Runtime in sec.
Beck et al. [4]	0	-0.04958	0.57116	1.88360	1.10466	0.47839	6
	1000	0.19091	0.14298	0.51528	0.30760	0.02459	14
	2000	0.26892	0.04361	0.15655	0.11004	0.01089	23
	3000	0.29646	0.01359	0.04874	0.03397	0.00724	31
	4000	0.30252	0.00584	0.02369	0.01444	0.01550	40
	5000	0.30584	0.00288	0.01243	0.00487	0.00662	49
Our results	0	-0.02988	0.58509	1.78238	1.27133	0.35253	2
	1000	0.20342	0.15110	0.48308	0.35003	0.01850	3
	2000	0.27478	0.04546	0.14750	0.10976	0.00412	5
	3000	0.29954	0.01301	0.03965	0.03319	0.00139	6
	4000	0.30582	0.00393	0.01328	0.00881	0.00120	7
	5000	0.30852	0.00123	0.00363	0.00184	0.00232	9

Figure 3: Relative L_1 approximation error and the mean of the empirical loss function of the 20-dimensional AC equation.

Example 2. Convolutional neural networks. We still utilize certain basic settings from Example 1, and the only thing that needs to be modified is the dimension of the data. Here, set $d = 256$ or $d = 400$.

Table 3: Numerical simulations of the large-dimensional AC equation.

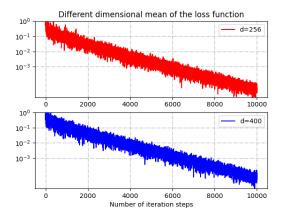| Dimension	Training steps	$\mu_{u^{\Theta_m}}$	$\sigma_{u^{\Theta_m}}$	$\mu_{L^1_{\text{error}}}$	$\sigma_{L^1_{\text{error}}}$	Mean of the loss function	Runtime in sec.
$d = 256$	0	-0.15151	0.57393	12.7026	7.15709	0.74728	2
	2000	0.03103	0.03149	0.73467	0.31448	0.02349	4
	4000	0.04045	0.00364	0.06574	0.06365	0.00616	7
	6000	0.04217	0.00131	0.02855	0.02033	0.00087	10
	8000	0.04139	0.00042	0.00797	0.00723	0.00010	12
	10000	0.04155	0.00011	0.00227	0.00158	0.00003	15
$d = 400$	0	0.08637	0.46341	14.6610	9.05968	0.32806	2
	2000	0.02730	0.01902	0.59862	0.36606	0.04361	4
	4000	0.02499	0.00474	0.16069	0.10427	0.00721	7
	6000	0.02685	0.00161	0.05114	0.03197	0.00239	10
	8000	0.02698	0.00082	0.02202	0.02099	0.00028	13
	10000	0.02729	0.00022	0.00850	0.00619	0.00004	15

Figure 4: Relative L_1 approximation error and the mean of the empirical loss function of the large-dimensional AC equation.

Table 3 extracts approximate solutions of u^{Θ_m} in different dimensions by convolutional neural networks. The difference with Example 1 is that the number of iteration steps here $m \in \{0, 2000, 4000, 6000, 8000, 10000\}$. And in Figure 4, $m \in \{0, 1, 2, \ldots, 10000\}$. Besides, the 256- and 400-dimensional value $u(0, \xi)$ of the solution u of the (34) has been replaced by the value 0.041531 and 0.027106, which is also calculated through the Branching diffusion method [25]. Hence, the different dimensional relative L_1-approximation error is calculated as $\dfrac{|u^{\Theta_m} - 0.041531|}{0.041531}, \dfrac{|u^{\Theta_m} - 0.027106|}{0.027106}$, respectively.

In Table 3 and Figure 4, no matter whether the dimension of the equation is 256 or 400, as the number of iteration steps increases, the relative L_1-approximation error of the approximate solution decreases gradually, and the loss function also tends to decrease in general. This shows that it is numerically feasible for us to use convolutional neural networks to approximately solve higher-dimensional stochastic PDEs.

4.2. High-dimensional BSB equation

This subsection presents the calculation of the high-dimensional BSB equation (see [2] and (38)). Similarly, we employ two examples to show that.

Example 3. Multiscale deep learning fusion. Suppose that $T = 1, d = 100, \tilde{d} \in \{75, 100, 50, 125\}, N = 20, \epsilon = 10^{-8}$, and assume for all $\omega \in \Omega$ that $\xi(\omega) = (1, \frac{1}{2}, 1, \frac{1}{2}, \ldots, 1, \frac{1}{2}) \in \mathbb{R}^d$. Set

$$\widetilde{\gamma}_m = 1.0 \cdot \left(\frac{1}{2}\right)^{[m/200]}. \tag{35}$$

Here, $[\cdot]$ represents taking the integer of $m/200$. By setting $\sigma_{max} = \frac{4}{10}$, $\sigma_{min} = \frac{1}{10}$, $\sigma_c = \frac{4}{10}$, let us define the function $\bar{\sigma} : \mathbb{R} \to \mathbb{R}$ as

$$\bar{\sigma}(x) = \begin{cases} \sigma_{max}, & x \geq 0, \\ \sigma_{min}, & x < 0 \end{cases} \tag{36}$$

for all $x \in \mathbb{R}$. Assuming for all $s, t \in [0, T]$, $\mathbf{x} = (\mathbf{x}_1, \ldots, \mathbf{x}_d)$, $\mathbf{w} = (\mathbf{w}_1, \ldots, \mathbf{w}_d)$, $\mathbf{z} = (\mathbf{z}_1, \ldots, \mathbf{z}_d) \in \mathbb{R}^d, y \in \mathbb{R}$, $S = (S_{ij})_{(i,j) \in \{1,\ldots,d\}^2} \in \mathbb{R}^{d \times d}$, we have that $\sigma(\mathbf{x}) = \sigma_c \text{diag}(\mathbf{x}_1, \ldots, \mathbf{x}_d), \mathcal{H}(s, t, \mathbf{x}, \mathbf{w}) = \mathbf{x} + \sigma(\mathbf{x})\mathbf{w}, \hat{g}(\mathbf{x}) = ||\mathbf{x}||_{\mathbb{R}^d}^2$, and that

$$f(t, \mathbf{x}, \mathbf{y}, \mathbf{z}, S) = -\frac{1}{2} \sum_{i=1}^{d} |\mathbf{x}_i|^2 |\bar{\sigma}(S_{ii})|^2 S_{ii} + \hat{r}(\mathbf{y} - \langle \mathbf{x}, \mathbf{z} \rangle_{\mathbb{R}^d}). \tag{37}$$

The solution $u : [0, T] \times \mathbb{R}^d \to \mathbb{R}$ such that $u(T, \mathbf{x}) = ||\mathbf{x}||_{\mathbb{R}^d}^2$ and

$$\frac{\partial u}{\partial t}(t, \mathbf{x}) + \frac{1}{2} \sum_{i=1}^{d} |\mathbf{x}_i|^2 |\bar{\sigma}(\frac{\partial^2 u}{\partial \mathbf{x}_i^2}(t, \mathbf{x}))|^2 \frac{\partial^2 u}{\partial \mathbf{x}_i^2}(t, \mathbf{x}) = \hat{r}(u(t, \mathbf{x}) - \langle \mathbf{x}, (\nabla_{\mathbf{x}} u)(t, \mathbf{x}) \rangle_{\mathbb{R}^d}) \tag{38}$$

for all $(t, \mathbf{x}) \in [0, T] \times \mathbb{R}^d$.

Table 4 lists different methods to approximatively calculate the mean and standard deviation of u^{Θ_m}, the mean and standard deviation of corresponding L_1-approximation error associated to u^{Θ_m}, and the runtime in seconds, needed to calculate one realization of u^{Θ_m} against $m \in \{0, 100, 200, 300, 400\}$ based on 10 independent runs. In addition, Figure 5 depicts approximations of the mean of the relative L_1-approximation error and approximations of the mean of the loss function associated to u^{Θ_m} against $m \in \{0, 1, 2, \ldots, 400\}$ based on 10 independent realizations. In the approximative calculations of the relative L^1-approximation error, the value $u(0, (1, \frac{1}{2}, 1, \frac{1}{2}, \ldots, 1, \frac{1}{2}))$ of the solution u of (38) has been replaced by the value 77.1049, in turn, which has been calculated by means of Lemma 4 below (more details see [4]). The relative L_1-approximation error is $\frac{|u^{\Theta_m} - 77.1049|}{77.1049}$.

Lemma 4. Suppose that $0 < c, \sigma_{max}, r, T < \infty$, $0 < \sigma_{min} < \sigma_{max}$, $d \in \mathbb{N}$, and assume $\bar{\sigma} : \mathbb{R} \to \mathbb{R}$ is the function, such that

$$\bar{\sigma}(x) = \begin{cases} \sigma_{max}, & x \geq 0, \\ \sigma_{min}, & x < 0 \end{cases} \tag{39}$$

for all $x \in \mathbb{R}$, and we let $\hat{g} : \mathbb{R}^d \to \mathbb{R}$ and $u : [0, T] \times \mathbb{R}^d \to \mathbb{R}$ be the functions, such that $\hat{g}(\mathbf{x}) = c||\mathbf{x}||_{\mathbb{R}^d}^2 = c \sum_{i=1}^{d} |\mathbf{x}_i|^2$ and

$$u(t, \mathbf{x}) = \exp([r + |\sigma_{max}|^2](T - t))\hat{g}(\mathbf{x}) \tag{40}$$

for all $t \in [0, T]$, $\mathbf{x} = (\mathbf{x}_1, \ldots, \mathbf{x}_d) \in \mathbb{R}^d$. Then, we have for all $t \in [0, T], \mathbf{x} = (\mathbf{x}_1, \ldots, \mathbf{x}_d) \in \mathbb{R}^d$ that $u \in C^\infty([0, T] \times \mathbb{R}^d, \mathbb{R}), u(T, \mathbf{x}) = \hat{g}(\mathbf{x})$, and

$$\frac{\partial u}{\partial t}(t, \mathbf{x}) + \frac{1}{2} \sum_{i=1}^{d} |\mathbf{x}_i|^2 |\bar{\sigma}(\frac{\partial^2 u}{\partial \mathbf{x}_i^2}(t, \mathbf{x}))|^2 \frac{\partial^2 u}{\partial \mathbf{x}_i^2}(t, \mathbf{x}) = \hat{r}(u(t, \mathbf{x}) - \langle \mathbf{x}, (\nabla_{\mathbf{x}} u)(t, \mathbf{x}) \rangle_{\mathbb{R}^d}). \tag{41}$$

Looking at Table 4 as a whole we observe that the approximate solution obtained by our method has higher accuracy. However, unlike Example 1, our runtime will be a bit more. Similarly, we paint Figure 5 for comparing with the existing methods. It is evident from Figure 5 that when the number of iteration steps exceeds 200, the proposed method already stratifies with the method of Beck et al. [4]. And from the partially enlarged picture, Beck et al. [4] method differs from us by one coordinate scale in terms of the relative L^1-approximation error and loss function value. These all demonstrate and illustrate the effectiveness of our method.

Table 4: Numerical simulations of the 100-dimensional BSB equation.

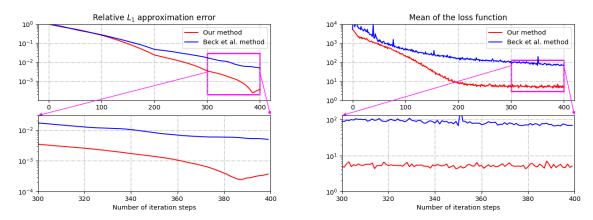| Method	Training steps	$\mu_{u^{\Theta_m}}$	$\sigma_{u^{\Theta_m}}$	$\mu_{L^1_{\text{error}}}$	$\sigma_{L^1_{\text{error}}}$	Mean of the loss function	Runtime in sec.
Beck et al. [4]	0	0.3940	0.2253	0.99489	0.00292	5355.51	23
	100	55.9301	1.9195	0.27462	0.02489	540.55	27
	200	73.4561	0.9547	0.04732	0.01238	149.26	31
	300	75.7877	0.5027	0.01708	0.00652	90.979	36
	400	76.7701	0.3009	0.00491	0.00316	63.846	40
Our results	0	0.5517	0.2378	0.99285	0.00308	5411.35	21
	100	57.0542	0.4246	0.26004	0.00551	226.89	29
	200	75.2420	0.1476	0.02416	0.00191	8.619	36
	300	76.8373	0.0515	0.00347	0.00067	4.866	44
	400	77.1226	0.0302	0.00039	0.00024	4.882	52

Figure 5: Relative L_1 approximation error and the mean of the empirical loss function of the 100-dimensional BSB equation.

Example 4. Convolutional neural networks. Herein, most of our settings are the same as Example 3. Based on this point, what needs to be modified is the dimension of the data and the learning rate. Firstly, we set $d = 256$ or $d = 400$, and the learning rate is
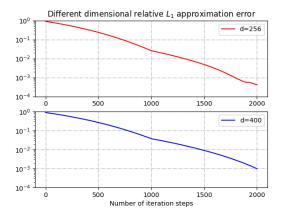
$$\widetilde{\gamma}_m = 2.0 \cdot \left(\frac{1}{2}\right)^{[m/500]}. \tag{42}$$

Table 5 reports approximate solutions of u^{Θ_m} in different dimensions by convolutional neural networks. The difference with Example 3 is that the number of iteration steps here $m \in \{0, 200, 400, 600, 800, 1000\}$. In addition, in Figure 6, $m \in \{0, 1, 2, \ldots, 1000\}$. Also, the 256- and 400-dimension value $u\left(0, (1, \frac{1}{2}, 1, \frac{1}{2}, \ldots, 1, \frac{1}{2})\right)$ of the solution u of (38) has been replaced via the value 197.3885 and 308.4195, respectively. It also can be computed by means of Lemma 4. And the different dimensions relative L_1-approximation error is $\frac{|u^{\Theta_m} - 197.3885|}{197.3885}$, $\frac{|u^{\Theta_m} - 308.4195|}{308.4195}$, respectively.

In Table 5, it can be seen that from 256 dimensions to 400 dimensions, the running time using convolutional neural networks increases exponentially. This is mainly because as the dimension increases, the memory overhead increases. However, the accuracy of the approximated solution did not change much. This demonstrates that convolutional neural networks can extend approximated solutions to higher dimensions without losing accuracy. Also, Figure 6 can show this more intuitively.

Table 5: Numerical simulations of the large-dimensional BSB equation.

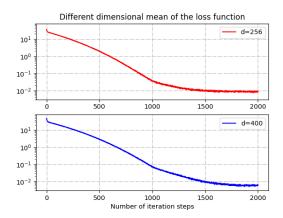| Dimension	Training steps	$\mu_{u^{\Theta_m}}$	$\sigma_{u^{\Theta_m}}$	$\mu_{L^1_{\text{error}}}$	$\sigma_{L^1_{\text{error}}}$	Mean of the loss function	Runtime in sec.
$d = 256$	0	0.4901	0.2948	0.99752	0.00149	35095	4
	200	164.3867	0.6826	0.16719	0.00346	345.59	34
	400	190.3597	0.2866	0.03561	0.00145	26.737	63
	600	194.5438	0.1614	0.01441	0.00082	17.643	92
	800	196.7375	0.1106	0.00330	0.00056	15.022	122
	1000	197.3413	0.0793	0.00041	0.00023	14.395	151
$d = 400$	0	0.5218	0.2603	0.99831	0.00084	86234	6
	200	170.3224	1.6187	0.44776	0.00525	3696.6	77
	400	271.3132	1.1839	0.12031	0.00384	347.57	148
	600	298.8917	0.6204	0.03089	0.00201	42.596	219
	800	305.8975	0.2641	0.00818	0.00086	29.087	291
	1000	308.5768	0.1068	0.00051	0.00035	23.190	362

Figure 6: Relative L_1 approximation error and the mean of the empirical loss function of the large-dimensional BSB equation.

4.3. High-dimensional HJB equation

This subsection approximatively calculates the solution of a high-dimensional HJB equation with a non-linearity that is quadratic in the gradient (see [25]). In the following, we present two examples to show the related calculation.

Example 5. Multiscale deep learning fusion. We suppose $d = 100, \tilde{d} \in \{50, 75, 100, 125\}, T = 1, N = 20, \epsilon = 10^{-8}$, and suppose for all $\omega \in \Omega$ that $\xi(\omega) = \mathbf{0} \in \mathbb{R}^d$. Then assume for all $m \in \mathbb{N}_0, s, t \in [0, T], \mathbf{x}, \mathbf{w}, \mathbf{z} \in \mathbb{R}^d, \mathbf{y} \in \mathbb{R}, S \in \mathbb{R}^{d \times d}$ that $\sigma(\mathbf{x}) = \sqrt{2}\mathrm{Id}_{\mathbb{R}^d}, \mathcal{H}(s, t, \mathbf{x}, \mathbf{w}) = \mathbf{x} + \sqrt{2}\mathbf{w}, \hat{g}(\mathbf{x}) = \ln\left(\frac{1}{2}[1 + ||\mathbf{x}||^2_{\mathbb{R}^d}]\right), f(t, \mathbf{x}, \mathbf{y}, \mathbf{z}, S) = -\mathrm{Trace}(S) - ||\mathbf{z}||^2_{\mathbb{R}^d}$, and

$$\widetilde{\gamma}_m = \frac{1}{100} \cdot \left(\frac{1}{5}\right)^{[m/1000]}. \tag{43}$$

The solution $u : [0, T] \times \mathbb{R}^d \to \mathbb{R}$ of the PDE (33) satisfies for all $(t, \mathbf{x}) \in [0, T) \times \mathbb{R}^d$ that

$$\frac{\partial u}{\partial t}(t, \mathbf{x}) + (\triangle_{\mathbf{x}} u) = ||\nabla_{\mathbf{x}} u(t, \mathbf{x})||^2_{\mathbb{R}^d}. \tag{44}$$
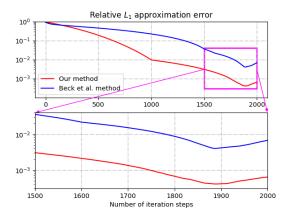
Table 6 lists different methods to approximatively calculate the mean and standard deviation of u^{Θ_m}, the mean and standard deviation of relative L_1-approximation error associated to u^{Θ_m}, and the runtime in seconds, needed to calculate one realization of u^{Θ_m} against $m \in \{0, 500, 1000, 1500, 2000\}$, based on 10

independent runs. Furthermore, Figure 7 shows approximations of the mean of the relative L_1-approximation error and approximations of the mean of the loss function associated to u^{Θ_m} against $m \in \{0, 1, 2, \ldots, 2000\}$ based on 10 independent realizations. For the approximative calculations of the relative L_1-approximation error, the value $u(0, \xi)$ of the solution u of (44) has been substituted by the value 4.5901, conversely, which was calculated by the means of in [25, Lemma 4.2] and the classical Monte Carlo method [25].

It can be clearly observed from Table 6 and Figure 7 that the approximated solution obtained via our method has higher accuracy. Figure 7, the curve slope of the relative L_1-approximation error and the loss function change with our method at 1000 steps, which is mainly caused by the change of the learning rate (see (43)). Likewise, we also place the local comparison from steps 1500 to 2000 at the bottom of this figure.

Table 6: Numerical simulations of the 100-dimensional HJB equation.

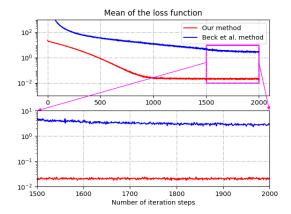| Method	Training steps	$\mu_{u^{\Theta_m}}$	$\sigma_{u^{\Theta_m}}$	$\mu_{L^1_{\text{error}}}$	$\sigma_{L^1_{\text{error}}}$	Mean of the loss function	Runtime in sec.
Beck et al. [4]	0	0.4328	0.0620	0.90571	0.01351	1065.5	17
	500	2.5108	0.0555	0.45300	0.01208	37.574	33
	1000	3.5726	0.0432	0.22168	0.00942	11.839	49
	1500	4.4255	0.0293	0.03587	0.00639	5.105	65
	2000	4.6101	0.0258	0.00673	0.00232	2.783	81
Our results	0	0.2294	0.0940	0.95001	0.02047	23.32	18
	500	3.7223	0.0603	0.18907	0.01313	0.834	42
	1000	4.5465	0.0097	0.00951	0.00212	0.025	67
	1500	4.5762	0.0052	0.00304	0.00113	0.022	91
	2000	4.5924	0.0021	0.00063	0.00024	0.019	115

Figure 7: Relative L_1 approximation error and the mean of the empirical loss function of the 100-dimensional HJB equation.

Example 6. Convolutional neural networks. Herein, certain basic settings from Example 5 are still used, and the only thing that needs to be changed is the dimension of the data. Below, set $d = 256$ or $d = 400$. Noting the learning rate, we adjusted the learning rate with a fixed number of steps instead of exponential decay. The specific formula is
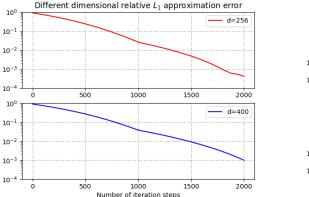
$$\widetilde{\gamma}_m = \begin{cases} 0.01, & m < 1000, \\ 0.005, & m \geq 1000. \end{cases} \tag{45}$$

Table 7 and Figure 8 display approximated solutions of u^{Θ_m} in different dimensions by convolutional neural networks. Besides, the 256- and 400-dimension value $u(0, \xi)$ of the solution u of (32) has been replaced by the value 5.5393 and 5.9877, which also can be calculated through the classical Monte Carlo method [25]. Thus, the different dimensions relative L_1-approximation error is $\frac{|u^{\Theta_m} - 5.5393|}{5.5393}$, $\frac{|u^{\Theta_m} - 5.9877|}{5.9877}$, respectively.

Comparing Table 6 and Table 7, one can find the fact that the running time of using convolutional neural network is faster than using linear neural network. Generally speaking, higher-dimensional problems require more memory and take longer to compute. While in Table 7, it only takes 7 seconds to calculate the 400-dimensional HJB equation. In addition, from the relative L_1-approximation error and loss function in Figure 8, the accuracy of the convolutional neural network is almost the same as that of the linear neural network. This shows that convolutional neural networks are more suitable than linear neural networks for the HJB equation.

Table 7: Numerical simulations of the large-dimensional HJB equation.

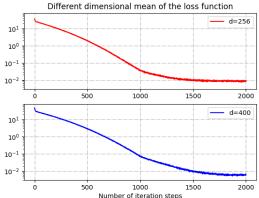| Dimension	Training steps	$\mu_{u\Theta_m}$	$\sigma_{u\Theta_m}$	$\mu_{L^1_{\text{error}}}$	$\sigma_{L^1_{\text{error}}}$	Mean of the loss function	Runtime in sec.
$d = 256$	0	0.5348	0.2753	0.90346	0.04970	35.86	1
	500	4.2221	0.1976	0.23779	0.03567	1.974	3
	1000	5.3966	0.0502	0.02576	0.00907	0.037	4
	1500	5.5126	0.0148	0.00481	0.00267	0.010	6
	2000	5.5399	0.0025	0.00042	0.00019	0.008	7
$d = 400$	0	0.5902	0.2538	0.90143	0.04239	48.68	2
	500	4.3749	0.1916	0.26935	0.03200	2.853	3
	1000	5.7611	0.0596	0.03784	0.00995	0.076	4
	1500	5.9330	0.0207	0.00913	0.00346	0.010	6
	2000	5.9818	0.0042	0.00099	0.00071	0.006	7

Figure 8: Relative L_1 approximation error and the mean of the empirical loss function of the large-dimensional HJB equation.

5. Summary

This paper developed numerical approximation for high-dimensional fully nonlinear merged PDEs and 2BS-DEs based on the deep CNN technique. First, the forward discretization was employed in the time direction, and then two approximation approaches were adopted in the space direction by the multi-scale deep learning fusion and the convolutional neural networks, from which, the former is more accurate and efficient than the method of Beck et al. [4]; the latter can use matrix arrangement to calculate higher-dimensional fully nonlinear PDEs, such as $d = 400$. These were reflected in the numerical experiments. Unfortunately, despite the computational improvement, we are temporarily unable to obtain theoretical results of the proposed methods, which will be further considered by us in the future. Following the results a future study will try to apply a temporal second-order approximation combined with a regularized convolutional neural network [57] for solving high-dimensional fully nonlinear merged PDEs-2BSDEs system, based on the stochastic pooling.

Declaration of competing interest

The authors have not disclosed any competing interests.

Data availability

No data was used for the research described in the article.

References

References

[1] A. L. Amadori, Nonlinear integro-differential evolution problems arising in option pricing: a viscosity solutions approach, Differential Integral Equations, 16 (2003), 787-811.

[2] M. Avellaneda, A. Levy, A. Parás, Pricing and hedging derivative securities in markets with uncertain volatilities, Appl. Math. Finance, 2 (1995), 73-88.

[3] E. Bayraktar, V. Young, Pricing options in incomplete equity markets via the instantaneous sharpe ratio, Ann. Finance, 4 (2008), 399-429.

[4] C. Beck, W. E, A. Jentzen, Machine learning approximation algorithms for high-dimensional fully nonlinear partial differential equations and second-order backward stochastic differential equations, J. Nonlinear Sci., 29 (2019), 1563-1619.

[5] C. Bender, R. Denk, A forward scheme for backward SDEs, Stochastic Process. Appl., 117 (2007), 1793-1812.

[6] C. Bender, N. Schweizer, J. Zhuo, A primal-dual algorithm for BSDEs, Math. Finance, 27 (2017), 866-901.

[7] Y. Bengio, Learning deep architectures for AI. Foundations and Trends in Machine Learning, 2 (2009), 1-127.

[8] B. Bouchard, R. Elie, N. Touzi, Discrete-time approximation of BSDEs and probabilistic schemes for fully nonlinear PDEs, In Advanced financial modelling (pp. 91-124), 2009. De Gruyter.

[9] B. Bouchard, N. Touzi, Discrete-time approximation and Monte-Carlo simulation of backward stochastic differential equations, Stochastic Process. Appl., 111 (2004), 175-206.

[10] P. Briand, C. Labart, Simulation of BSDEs by Wiener chaos expansion, Ann. Appl. Probab., 24 (2014), 1129-1171.

[11] G. Carleo, M. Troyer, Solving the quantum many-body problem with artificial neural networks, Science, 355 (2017), 602-606.

[12] D. Chang, H. Liu, J. Xiong, A branching particle system approximation for a class of FBSDEs, Probab. Uncertain. Quant. Risk, 1 (2016), 1-34.

[13] J. F. Chassagneux, Linear multistep schemes for BSDEs, SIAM J. Numer. Anal., 52 (2014), 2815-2836.

[14] J. F. Chassagneux, D. Crisan, Runge-Kutta schemes for backward stochastic differential equations, Ann. Appl. Probab., 24 (2014), 679-720.

[15] J. F. Chassagneux, A. Richou, Numerical stability analysis of the Euler scheme for BSDEs, SIAM J. Numer. Anal., 53 (2015), 1172-1193.

[16] J. F. Chassagneux, A. Richou, A. Numerical simulation of quadratic BSDEs, Ann. Appl. Probab., 26 (2016), 262-304.

[17] P. Cheridito, H. M. Soner, N. Touzi, N. Victoir, Second-order backward stochastic differential equations and fully nonlinear parabolic PDEs. Comm. Pure Appl. Math., 60 (2007), 1081-1110.

[18] S. Crépey, R. Gerboud, Z. Grbac, N. Ngor, Counterparty risk and funding: The four wings of the TVA, Int. J. Theor. Appl. Finance, 16 (2013), 1350006.

[19] D. Crisan, K. Manolarakis, Solving backward stochastic differential equations using the cubature method: application to nonlinear pricing, SIAM J. Financial Math., 3 (2012), 534-571.

[20] D. Crisan, K. Manolarakis, Second order discretization of backward SDEs and simulation with the cubature method, Ann. Appl. Probab., 24 (2014), 652-678.

[21] D. Crisan, K. Manolarakis, N. Touzi, On the Monte Carlo simulation of BSDEs: an improvement on the Malliavin weights, Stochastic Process. Appl., 120 (2010), 1133-1158.

[22] J. Darbon, S. Osher, Algorithms for overcoming the curse of dimensionality for certain Hamilton-Jacobi equations arising in control theory and elsewhere, Res. Math. Sci., 3 (2016), 1-26.

[23] F. Delarue, S. Menozzi, A forward-backward stochastic algorithm for quasi-linear PDEs, Ann. Appl. Probab., 16 (2006), 140-184.

[24] Jr. J. Douglas, J. Ma, P. Protter, Numerical methods for forward-backward stochastic differential equations, Ann. Appl. Probab., 6 (1996), 940-968.

[25] W. E, J. Han, A. Jentzen, Deep learning-based numerical methods for high-dimensional parabolic partial differential equations and backward stochastic differential equations, Commun. Math. Stati., 5 (2017), 349-380.

[26] Y. Fu, W. Zhao, T. Zhou, Efficient spectral sparse grid approximations for solving multi-dimensional forward backward SDEs, Discrete Contin. Dyn. Syst. Ser. B, 22 (2017), 3439-3458.

[27] E. Gobet, C. Labart, Solving BSDE with adaptive control variate, SIAM J. Numer. Anal. 48 (2010), 257-277.

[28] E. Gobet, J. P. Lemor, Numerical simulation of BSDEs using empirical regression methods: theory and practice, arXiv:0806.4447 (2008), 17 pages.

[29] E. Gobet, J. P. Lemor, X. Warin, A regression-based Monte Carlo method to solve backward stochastic differential equations, Ann. Appl. Probab., 15 (2005), 2172-2202.

[30] E. Gobet, J. G. López-Salas, P. Turkedjiev, C. Vázquez, Stratified regression Monte-Carlo scheme for semilinear PDEs and BSDEs with large scale parallelization on GPUs, SIAM J. Sci. Comput, 38 (2016), C652-C677.

[31] E. Gobet, P. Turkedjiev, Linear regression MDP scheme for discrete backward stochastic differential equations under general conditions. Math. Comput., 85 (2016), 1359-1391.

[32] W. Guo, J. Zhang, J. Zhuo, A monotone scheme for high-dimensional fully nonlinear PDEs, Ann. Appl. Probab., 25 (2015), 1540-1580.

[33] J. Han, A. Jentzen, W. E, Overcoming the curse of dimensionality: Solving high-dimensional partial differential equations using deep learning, Proceedings of the National Academy of Sciences, 115 (2018), 8505-8510.

[34] P. Henry-Labordère, X. Tan, N. Touzi, A numerical algorithm for a class of BSDEs via the branching process, Stochastic Process. Appl., 124 (2014), 1112-1140.

[35] J. Hu, Z. Chen, M. Yang, R. Zhang, Y. Cui, A multiscale fusion convolutional neural network for plant leaf recognition, IEEE Signal Processing Letters, 25 (2018), 853-857.

[36] T. P. Huijskens, M. J. Ruijter, C. W. Oosterlee, Efficient numerical Fourier methods for coupled forward-backward SDEs, J. Comput. Appl. Math., 296 (2016), 593-612.

[37] D. Kingma, J. Ba, Adam: a method for stochastic optimization, Proceedings of the International Conference on Learning Representations (ICLR), May 2015.

[38] P. E. Kloeden, E. Platen, Numerical solution of stochastic differential equations, vol. 23 of Applications of Mathematics (New York). Springer-Verlag, Berlin, 1992.

[39] S. G. Kong, J. Heo, F. Boughorbel et al., Multiscale fusion of visible and thermal IR images for illumination-invariant face recognition, Int. J. Comput. Vision, 71 (2007), 215-233.

[40] T. Kong, W. Zhao, T. Zhou, Probabilistic high order numerical schemes for fully nonlinear parabolic PDEs, Commun. Comput. Phys., 18 (2015), 1482-1503.

[41] Y. LeCun, Y. Bengio, G. Hinton, Deep learning, Nature 521 (2015), 436-444.

[42] Y. Lecun, L. Bottou, Y.Bengio, P. Haffner, Gradient-based learning applied to document recognition, Proceedings of the IEEE, 86 (1998), 2278-2324.

[43] H. Lee, I. S. Kang, Neural algorithm for solving differential equations, J. Comput. Phys. 91 (1990), 110-131.

[44] J. Long, E. Shelhamer, T. Darrell, Fully convolutional networks for semantic segmentation, In Proceedings of the IEEE conference on computer vision and pattern recognition (CVPR), (2015), 3431-3440.

[45] J. Ma, P. Protter, J. San Martín, S. Torres, Numerical method for backward stochastic differential equations, Ann. Appl. Probab., 12 (2002), 302-316.

[46] J. Ma, J. Yong, Forward-backward stochastic differential equations and their applications, vol. 1702 of Lecture Notes in Mathematics, Springer-Verlag, Berlin, 1999.

[47] G. N. Milstein, M. V. Tretyakov, Numerical algorithms for forward-backward stochastic differential equations, SIAM J. Sci. Comput., 28 (2006), 561-582.

[48] G. N. Milstein, M. V. Tretyakov, Discretization of forward-backward stochastic differential equations and related quasi-linear parabolic equations, IMA J. Numer. Anal., 27 (2007), 24-44.

[49] B. Oksendal, Stochastic differential equations: an introduction with applications, Springer Science & Business Media, 2013.

[50] E. Pardoux, S. Peng, Adapted solution of a backward stochastic differential equation, Systems Control Lett., 14 (1990), 55-61.

[51] E. Pardoux, S. Tang, Forward-backward stochastic differential equations and quasilinear parabolic PDEs, Probab. Theory Related Fields, 114 (1999), 123-150.

[52] S. Peng, G-expectation, G-Brownian motion and related stochastic calculus of Itô type, In Stochastic analysis and applications, 2 (2007), 541-567.

[53] H. Pham, Feynman-Kac representation of fully nonlinear PDEs and applications, Acta Math. Vietnam., 40 (2015), 255-269.

[54] P. Ramuhalli, L. Udpa, S. S. Udpa, Finite-element neural networks for solving differential equations, IEEE Trans. Neur. Netw., 16 (2005), 1381-1392.

[55] O. Ronneberger, P. Fischer, T. Brox, U-net: Convolutional networks for biomedical image segmentation. In International Conference on Medical image computing and computer-assisted intervention, (2015), 234-241.

[56] Y. K. Wang, C. T. Fan, Single image defogging by multiscale depth fusion, IEEE Trans. imag. process., 23 (2014), 4826-4837.

[57] M. D. Zeiler, R. Fergus, Stochastic pooling for regularization of deep convolutional neural networks, arXiv preprint arXiv:1301.3557, 2013.